

AD-A174 831

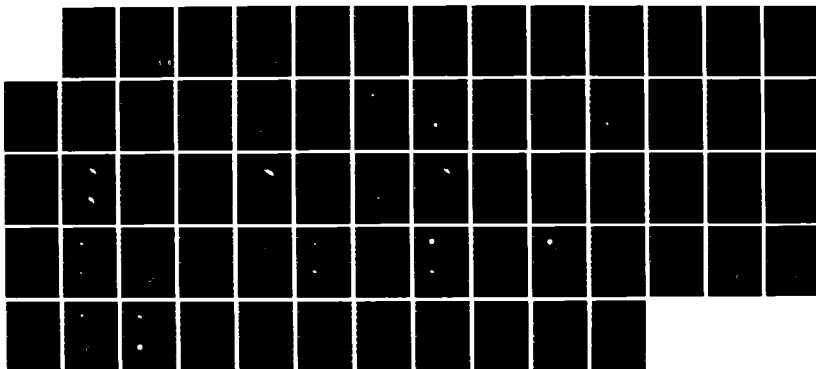
ON THE PREDICTION OF HIGHLY VORTICAL FLOWS USING AN
EULER EQUATION MODEL... (U) GRUMMAN CORP BETHPAGE NY
CORPORATE RESEARCH CENTER F MARCONI 03 FEB 86 RE-713
AFOSR-TR-86-2073 F49620-84-C-0056

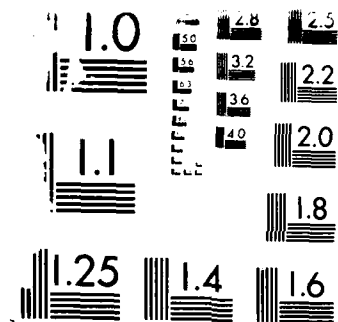
1/1

UNCLASSIFIED

F/G 20/4

NL





12. RESOLUTION TEST CHART
 1010-10A

2

AFOSR-TR. 86-2073

Approved for public release;
distribution unlimited.

REPORT RE-713

ON THE PREDICTION OF HIGHLY VORTICAL
FLOWS USING AN EULER EQUATION MODEL

DECEMBER 1985

prepared by

Frank Marconi
Fluid Mechanics Directorate

Corporate Research Center
Grumman Corporation
Bethpage, NY 11714

Final Report on
Contract F49620-84-C-0056

prepared for

USAF Office of Scientific Research
Building 410
Bolling AFB, DC 20332

AIR FORCE
NOTES
This report was prepared for the
AFOSR-TR-86-2073 project and is
discussed in AFOSR-TR-86-2073-12.
MATTHEW J. KENNEDY
Chief, Technical Information Division

SEARCH (AFSC)

AD-A174 831

DTIC FILE COPY

DTIC
ELECTE
DEC 02 1986
S D

86 11 25 379

UNCLASSIFIED

SECURITY CLASSIFICATION OF THIS PAGE

REPORT DOCUMENTATION PAGE

1a. REPORT SECURITY CLASSIFICATION UNCLASSIFIED		1b. RESTRICTIVE MARKINGS NONE													
2a. SECURITY CLASSIFICATION AUTHORITY		3. DISTRIBUTION/AVAILABILITY OF REPORT APPROVED FOR PUBLIC RELEASE; DISTRIBUTION UNLIMITED													
2b. DECLASSIFICATION/DOWNGRADING SCHEDULE															
4. PERFORMING ORGANIZATION REPORT NUMBER(S)		5. MONITORING ORGANIZATION REPORT NUMBER(S) AFOSR-TR- 86-2073													
6a. NAME OF PERFORMING ORGANIZATION Grumman Aerospace Corporation	6b. OFFICE SYMBOL (If applicable)	7a. NAME OF MONITORING ORGANIZATION Air Force Office of Scientific Research													
6c. ADDRESS (City, State, and ZIP Code) Mail Stop A08-35 Corporate Research Center Bethpage, New York 11714		7b. ADDRESS (City, State, and ZIP Code) Bolling AFB, Building 410 Bolling AFB, Washington, DC 20332													
8a. NAME OF FUNDING SPONSORING ORGANIZATION SAME	8b. OFFICE SYMBOL (If applicable) NA	9. PROCUREMENT INSTRUMENT IDENTIFICATION NUMBER													
8c. ADDRESS (City, State, and ZIP Code) SAME AFOSR/NA Bolling AFB, DC 20332		10. SOURCE OF FUNDING NUMBERS <table border="1"><tr><td>PROGRAM ELEMENT NO 61102F</td><td>PROJECT NO 2307</td><td>TASK NO A1</td><td>WORK UNIT ACCESSION NO</td></tr></table>		PROGRAM ELEMENT NO 61102F	PROJECT NO 2307	TASK NO A1	WORK UNIT ACCESSION NO								
PROGRAM ELEMENT NO 61102F	PROJECT NO 2307	TASK NO A1	WORK UNIT ACCESSION NO												
11. TITLE (Include Security Classification) On the Prediction of Highly Vortical Flows Using an Euler Equation Model															
12. PERSONAL AUTHOR(S) Frank Marconi															
13a. TYPE OF REPORT FINAL	13b. TIME COVERED FROM 6/13/84 TO 6/15/85	14. DATE OF REPORT (Year, Month, Day) 3 FEB -86	15. PAGE COUNT												
16. SUPPLEMENTARY NOTATION															
17. COSATI CODES <table border="1"><tr><td>FIELD</td><td>GROUP</td><td>SUB-GROUP</td></tr><tr><td></td><td></td><td></td></tr><tr><td></td><td></td><td></td></tr><tr><td></td><td></td><td></td></tr></table>		FIELD	GROUP	SUB-GROUP										18. SUBJECT TERMS (Continue on reverse if necessary and identify by block number) Fluid Mechanics Vortex Flows Supersonic Flows	
FIELD	GROUP	SUB-GROUP													
19. ABSTRACT (Continue on reverse if necessary and identify by block number) <p>An investigation of the power of the Euler equations in the prediction of conical separated flows is presented. These equations are solved numerically for the highly vortical supersonic flow about circular and elliptic cones. Two sources of vorticity are studied; the first is the flow field shock system and the second is the vorticity shed into the flow field from a separating boundary layer. Both sources of vorticity are found to produce separation and vortices. In the case of shed vorticity, the surface point from which the vorticity is shed (i.e., separation point) is determined empirically. Solutions obtained with both sources of vorticity are studied in detail, compared with each other, and with potential calculations and experimental data.</p>															
20. DISTRIBUTION/AVAILABILITY OF ABSTRACT <input type="checkbox"/> UNCLASSIFIED/UNLIMITED <input type="checkbox"/> SAME AS RPT <input type="checkbox"/> DTIC USERS		21. ABSTRACT SECURITY CLASSIFICATION													
22a. NAME OF RESPONSIBLE INDIVIDUAL DR JAMES D WILSON		22b. TELEPHONE (Include Area Code) 202-767-4935	22c. OFFICE SYMBOL NA												

DD FORM 1473, 84 MAR

83 APR edition may be used until exhausted
All other editions are obsolete

SECURITY CLASSIFICATION OF THIS PAGE

UNCLASSIFIED

REPORT RE-713

ON THE PREDICTION OF HIGHLY VORTICAL
FLOWS USING AN EULER EQUATION MODEL

DECEMBER 1985

prepared by

Frank Marconi
Fluid Mechanics Directorate

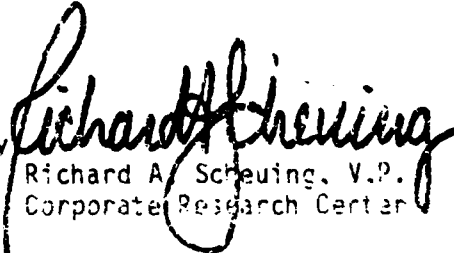
Corporate Research Center
Grumman Corporation
Bethpage, NY 11714

Final Report on
Contract F49620-84-C-0056

prepared for

USAF Office of Scientific Research
Building 410
Bolling AFB, DC 20332

Approved by


Richard A. Scheuing, V.P.
Corporate Research Center

SUMMARY

An investigation of the power of the Euler equations in the prediction of conical separated flows is presented. These equations are solved numerically for the highly vortical supersonic flow about circular and elliptic cones. Two sources of vorticity are studied; the first is the flow field shock system and the second is the vorticity shed into the flow field from a separating boundary layer. Both sources of vorticity are found to produce separation and vortices. In the case of shed vorticity, the surface point from which the vorticity is shed (i.e., separation point) is determined empirically. Solutions obtained with both sources of vorticity are studied in detail, compared with each other, and with potential calculations and experimental data.

TABLE OF CONTENTS

<u>Section</u>	<u>Page</u>
1. INTRODUCTION.....	1
2. COMPUTATIONAL PROCEDURE.....	5
3. COMPUTATIONAL RESULTS - SHOCK INDUCED VORTICITY.....	9
4. SHED VORTICITY - COMPUTATIONAL MODEL.....	29
5. COMPUTATIONAL RESULTS - SHED VORTICITY.....	35
5. COMPARISON OF SHOCK VORTICITY & SHED VORTICITY.....	51
7. CONCLUSIONS.....	57
8. REFERENCES.....	59



Accession For	
NTIS CRA&I	<input checked="" type="checkbox"/>
DTIC TAB	<input type="checkbox"/>
Unannounced	<input type="checkbox"/>
Justification	
By	
Distribution /	
Availability Codes	
Dist	Avail and/or Special
A-1	

LIST OF ILLUSTRATIONS

Figure		Page
1	Three-Dimensional Sketch of Flow Field & Coordinate System...	4
2	Comparison of Computation with Two Grids, Surface Pressure ($M_\infty = 2$, $\delta = 10^\circ$, $\alpha = 25^\circ$).....	10
3	Cross Flow Streamlines in Field ($M_\infty = 2$, $\delta = 10^\circ$, $\alpha = 25^\circ$)...	10
4	Cross Flow Streamlines Near Lee Plane ($M_\infty = 2$, $\delta = 10^\circ$, $\alpha = 25^\circ$).....	12
5	Surface Cross Flow Velocity ($M_\infty = 2$, $\delta = 10^\circ$, $\alpha = 25^\circ$).....	12
6	Isobars in Cross Plane ($M_\infty = 2$, $\delta = 10^\circ$, $\alpha = 25^\circ$).....	13
7	Lines of Constant Radial Vorticity X Spherical Radius ($M_\infty = 2$, $\delta = 10^\circ$, $\alpha = 25^\circ$).....	13
8	Inviscid Shock Induced Separation Point Location vs Shock Strength ($M_\infty = 2$, $\delta = 10^\circ$).....	16
9	Cross Flow Streamlines Near Lee Plane ($M_\infty = 3$, $\delta = 9.46^\circ$, $\alpha = 25^\circ$).....	16
10	Isobars Near Lee Plane ($M_\infty = 3$, $\delta = 9.46^\circ$, $\alpha = 25^\circ$).....	17
11	Surface Pressure Comparison ($M_\infty = 3$, $\delta = 9.46^\circ$, $\alpha = 25^\circ$).....	17
12	Surface Pressure Comparison ($M_\infty = 4.25$, $\delta = 5^\circ$, $\alpha = 12.35^\circ$)..	19
13	Isobars Near Leading Edge & Shock ($M_\infty = 2$, $\alpha = 10^\circ$, Ellipse, $\delta = 2.08^\circ$, $\lambda = 70^\circ$).....	21
14	Isobars Near Leading Edge & Shock ($M_\infty = 1.97$, $\alpha = 10^\circ$, 6:1 Ellipse, $\delta = 3.17^\circ$, $\lambda = 71.61^\circ$).....	21
15	Entropy Distribution Along the Shock (10:1 Ellipse, $M_\infty = 2$, $\alpha = 10^\circ$, $\delta = 2.08^\circ$, $\lambda = 70^\circ$) (6:1 Ellipse, $M_\infty = 1.97$, $\alpha = 10^\circ$, $\delta = 3.17^\circ$, $\lambda = 71.61^\circ$) (Cone, $M_\infty = 2$, $\alpha = 25^\circ$, $\delta = 10^\circ$).....	22
16	Surface Crossflow Mach Number Distribution (10:1 Ellipse, $M_\infty = 2$, $\alpha = 10^\circ$, $\delta = 2.08^\circ$, $\lambda = 70^\circ$) (6:1 Ellipse, $M_\infty = 1.97$, $\alpha = 10^\circ$, $\delta = 3.17^\circ$, $\lambda = 71.61^\circ$) (Cone, $M_\infty = 2$, $\alpha = 25^\circ$, $\delta = 10^\circ$).....	22
17	Isobars Near Leading Edge & Shock ($M_\infty = 2$, $\alpha = 10^\circ$, 14:1 Ellipse, $\delta = 1.5^\circ$, $\lambda = 70^\circ$).....	24

18	Surface Pressure Comparison ($M_\infty = 2$, $\alpha = 10^\circ$, 14:1 Ellipse, $\delta = 1.5^\circ$, $\lambda = 70^\circ$).....	24
19	Crossflow Streamlines ($M_\infty = 2$, $\alpha = 10^\circ$, 10:1 Ellipse, $\delta = 1.86^\circ$, $\lambda = 72^\circ$).....	26
20	Crossflow Streamlines Near Leading Edge ($M_\infty = 2$, $\alpha = 10^\circ$, 10:1 Ellipse, $\delta = 1.86^\circ$, $\lambda = 72^\circ$).....	26
21	Isobars Near Leading Edge ($M_\infty = 2$, $\alpha = 10^\circ$, 10:1 Ellipse, $\delta = 1.86^\circ$, $\lambda = 72^\circ$).....	27
22	Surface Pressure Comparison ($M_\infty = 2$, $\alpha = 10^\circ$, 10:1 Ellipse, $\delta = 1.86^\circ$, $\lambda = 72^\circ$).....	27
23	Sketch of Forced Separation Model.....	31
24	Cross Flow Streamlines, Primary Separation ($M_\infty = 1.79$, $\delta = 5^\circ$, $\alpha = 12.65^\circ$).....	37
25	Cross Flow Streamlines, Primary & Secondary Separations ($M_\infty = 1.79$, $\delta = 5^\circ$, $\alpha = 12.65^\circ$).....	37
26	Surface Crossflow Velocity Distribution, Primary and Secondary Separations ($M_\infty = 1.79$, $\delta = 5^\circ$, $\alpha = 12.65^\circ$).....	38
27	Surface Pressure Comparison ($M_\infty = 1.79$, $\delta = 5^\circ$, $\alpha = 12.65^\circ$)..	38
28	Surface Pressure Comparison ($M_\infty = 1.79$, $w = 5^\circ$, $\alpha = 10.6^\circ$)...	40
29	Crossflow Streamlines, Primary & Secondary Separations ($M_\infty = 1.79$, $\delta = 5^\circ$, $\alpha = 10.6^\circ$).....	40
30	Crossflow Streamlines, Primary Separation ($M_\infty = 1.79$, $\delta = 5^\circ$, $\alpha = 10.6^\circ$).....	41
31	Crossflow Streamlines, Forced Primary Separation Shock Induced Secondary Separation ($M_\infty = 4.25$, $\delta = 5^\circ$, $\alpha = 12.35^\circ$)	41
32	Isobars, Forced Primary Separation, Shock Induced Secondary Separation ($M_\infty = 4.25$, $\delta = 5^\circ$, $\alpha = 12.35^\circ$).....	43
33	Crossflow Streamlines, Forced Primary and Secondary Separations ($M_\infty = 4.25$, $\delta = 5^\circ$, $\alpha = 12.35^\circ$).....	43
34	Isobars, Forced Primary and Secondary Separations ($M_\infty = 4.25$, $\delta = 5^\circ$, $\alpha = 12.35^\circ$).....	45
35	Crossflow Sonic Lines, Forced Primary and Secondary Separations ($M_\infty = 4.25$, $\delta = 5^\circ$, $\alpha = 12.35^\circ$).....	45
36	Surface Pressure Comparison ($M_\infty = 4.25$, $\delta = 5^\circ$, $\alpha = 12.35^\circ$)..	46

37	Surface Pressure Comparison ($M_\infty = 2$, $\alpha = 10^\circ$, 14:1 Ellipse, $\delta = 1.5^\circ$, $\lambda = 70^\circ$) Separation Forced at $X/X_{LE} = .99$	46
38	Crossflow Streamlines ($M_\infty = 2$, $\alpha = 10^\circ$, 14:1 Ellipse, $\delta = 1.5^\circ$, $\lambda = 70^\circ$) Separation Forced at $X/X_{LE} = .99$	48
39	Isobars ($M_\infty = 2$, $\alpha = 10^\circ$, 14:1 Ellipse, $\delta = 1.5^\circ$, $\lambda = 70^\circ$) Separation Forced at $X/X_{LE} = .99$	48
40	Surface Pressure Comparison ($M_\infty = 2$, $\alpha = 10^\circ$, 14:1 Ellipse, $\delta = 1.5^\circ$, $\lambda = 70^\circ$) Separation Forced at $X/X_{LE} = .99$ and $X/X_{LE} = .8$	49
41	Crossflow Streamlines ($M_\infty = 2$, $\alpha = 10^\circ$, 14:1 Ellipse, $\delta = 1.5^\circ$, $\lambda = 70^\circ$) Separation Forced at $X/X_{LE} = .99$ and $X/X_{LE} = .8$	49
42	Crossflow Streamlines on the 5° Circular Cone ($M_\infty = 4.25$, $\alpha = 12.35^\circ$) Separation Due to Shock Vorticity Alone at $\theta = 151.3^\circ$	52
43	Isobars on the 5° Circular Cone ($M_\infty = 4.25$, $\alpha = 12.35^\circ$) Separation due to Shock Vorticity Alone at $\theta = 151.3^\circ$	52
44	Crossflow Streamlines on the 5° Circular Cone ($M_\infty = 4.25$, $\alpha = 12.35^\circ$) Separation Forced at $\theta = 115^\circ$	53
45	Isobars on the 5° Circular Cone ($M_\infty = 4.25$, $\alpha = 12.35^\circ$) Separation Forced at $\theta = 115^\circ$	53
46	Vorticity Shed into the Flow Field as a Function of Separation Point Location.....	54

INTRODUCTION

Separation and the formation of vortices in the three-dimensional flow about wings and forebodies at high angles of attack is an important aspect of advanced vehicle design. The phenomenon will be especially important at maneuver conditions for the next generation fighter aircraft since the flight envelopes of these vehicles may extend to high angles of attack at supersonic speeds. An understanding of three-dimensional separation and accompanying vortex formation may help in adding to the aerodynamic efficiency of these aircraft. Design efforts which try to take advantage of vortex lift or utilize vortex flaps will surely benefit from basic studies of separated flows. Controllability problems associated with vortex interactions and asymmetric forebody separation will benefit from an understanding of flow separation. If separated flows can be studied accurately and efficiently using computational techniques, the development costs of these aircraft will be significantly reduced.

This paper presents a numerical study of separation and accompanying vortices in the flow about delta wings and circular forebodies at supersonic speeds. The governing equations considered in this investigation are inviscid (i.e., Euler's equation). It is well known that separation zones (i.e., spirals or closed separation bubbles in 2-D flow) are associated with the existence of vorticity in the flow^{1,2,3,4}. There are two sources of vorticity in the high Reynolds number flows about supersonic aircraft: first, the vorticity in the boundary layer and second, the vorticity produced by shock waves. When boundary layer separation occurs, the vorticity of the boundary layer is shed into the flow field and may, to a good approximation, be considered as confined to an infinitesimal sheet which rolls into a vortex. This approximation has been used in conjunction with linearized flow field models for many years (see, for example, Ref. 5 and 6) with good results. The present author⁷ showed preliminary Euler calculations which indicated that the more exact flow field model made the computation of vortex flows simpler and at the same time more accurate. At flight Reynolds numbers ($> 10^6$), viscous effects are confined to thin flow regimes (boundary layers and vortex sheets) with the majority of the flow inviscid in nature. This fact makes the solution of the Navier-Stokes equations with a unified procedure (no special

treatment of sheets or boundary layers) very difficult. The Euler equations combined with special treatments for sheets and boundary layer may turn out to be a more reliable and accurate approach to the prediction of these flows. The power of the Euler equation model lies in its ability to transport vorticity while avoiding the evaluation of viscous terms. The extent of the capability of the Euler equations to predict separated flows is a major goal of this work.

In the past few years a number of investigators have studied numerical solutions to the Euler equations exhibiting separation. In Ref. 8, Salas showed how shock vorticity can cause separation at the base of a cylinder. Rizzi et al⁹ and Murman¹⁰ have shown solutions to Euler's equations with leading edge separation. In Ref. 9 and 10, the source of vorticity is unclear; there is no evidence of strong shock waves. Both authors indicate the possibility that separation is caused by numerical viscosity. In Ref. 10, the wing is a flat plate delta; therefore, there must be a singularity at the leading edge. The numerical scheme used could implicitly introduce a Kutta condition at the leading edge and shed vorticity into the flow field. R. Newsome¹¹ showed Euler solutions over an elliptic delta wing with finite thickness. His crude grid results exhibited leading edge separation (before any crossflow shock); his very fine grid results exhibited separation after a crossflow shock. The numerical schemes of Ref. 9, 10, and 11 require the addition of artificial viscosity for stability. Their research has indicated a small sensitivity of separation zones to reductions in artificial viscosity. It could be that these separation zones are Reynolds number independent (even numerical Reynolds number independent) and only zero artificial viscosity will keep the flow attached. It is interesting to note that the separated flows of Ref. 9, 10, and 11 compare well (at least qualitatively) with experimental data even though the source of vorticity is numerical (artificial viscosity or truncation error) in nature.

In the Euler calculations presented here, separation occurs only when a well defined source of vorticity is present. In addition to vorticity shed from the boundary layer, shock waves in supersonic conical flow can produce enough vorticity to induce separation. This type of separation is qualitatively similar to that produced by vorticity shed from a boundary layer. With boundary layer vorticity excluded, any comparison with

experimental data will be poor. It is difficult to assess the relative magnitude of the vorticity introduced into the flow from shocks and the boundary layer. It should be pointed out that experimental data show large regions of separated flow with no significant shock vorticity. This seems to indicate that vorticity shed from the boundary layer is much larger than that produced by shocks. In addition, boundary layer separation has a tendency to reduce shock strengths and therefore shock vorticity. Nevertheless, shock vorticity may still play an important role in the separation process. Additionally, the investigation of shock vorticity induced separation can shed some light on separated flow in general. The author investigated the effects of shock vorticity on circular cones^{7,12} and on elliptic delta wings¹³ and found that at high angle of attack a crossflow shock (Fig. 1) can produce enough vorticity to cause separation. This phenomenon will be discussed in detail later in this paper.

All geometries considered in this work are either delta wings which are elliptic in cross section or circular cones. In addition, each section normal to the z axis (Fig. 1) is self similar so that the geometry is conical. The flow is assumed supersonic everywhere and separation lines are assumed to be on conical rays. With these assumptions and that of a conical body, it follows that the flow is conical (i.e., all flow variables are independent of the spherical radius r (Fig. 1)). However, the basic features of the flow, including separation and vortices, are three-dimensional in nature.

In this paper our previous work in highly vortical flows^{7,12,13} will be reviewed after which our more recent findings will be presented. The overall computational procedure will be outlined and the model for shedding vorticity from specified separation points will be discussed. Flow fields with shock vorticity induced separation will be studied, in addition to flows with vorticity shed from both primary and secondary boundary layer separation points. A detailed comparison of these two different sources of vorticity will be presented. The investigation of the computed flow fields will be aided by comparisons with experimental data and computations of other researchers, including potential flow results. Finally, the findings of this work to date will be summarized.

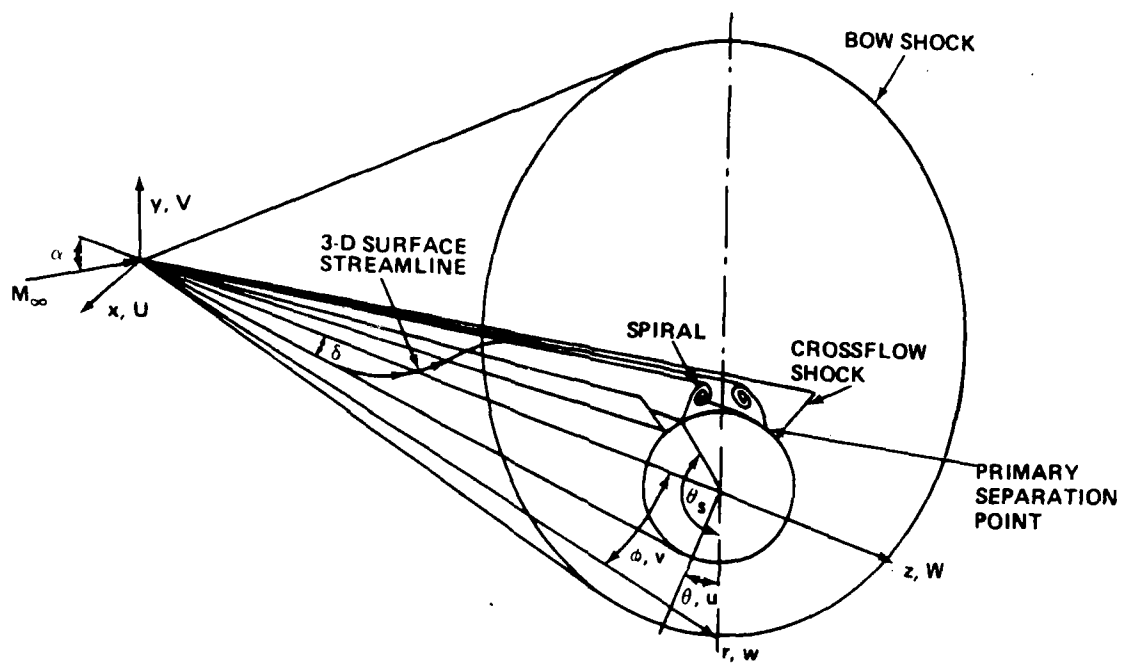


Fig. 1 Three-Dimensional Sketch of Flow Field & Coordinate System

2. COMPUTATIONAL PROCEDURE

The overall numerical procedure used in this study, although employing a number of new features, is essentially standard.¹⁴ The fully three-dimensional Euler's equations are solved with an explicit marching technique. The marching direction, z (Fig. 1), is an iterative coordinate for the conical flow considered here. The scheme is restricted by the fact that the axial component of velocity, W , (Fig. 1), must be supersonic everywhere. The marching scheme is continued until the flow field is invariant with respect to the computational marching direction except for a scale factor. The finite difference scheme used is Moretti's characteristic based λ -scheme.¹⁵ The bow shock and the primary crossflow shock are fit and are forced to satisfy the exact Rankine-Hugoniot jump conditions. The bow shock is fit as the outermost boundary of the flow field. On the low pressure side of the bow shock, freestream conditions exist. The crossflow shock is fit as an internal boundary of the flow field with its low pressure side being computed as the computation proceeds.¹⁶

The crossflow shock computation is a critical part of the overall procedure, particularly since it plays such a critical role in separation. As mentioned in the Introduction, it is the vorticity produced by the crossflow shock which is significant. Any scheme that captures the crossflow shock and introduces additional artificial viscosity to stabilize it runs the risk of distorting the separation and vortex. The bow shock also introduces vorticity into the flow field but not enough to produce separation. The crossflow shock is caused by the fact that at a large incidence the crossflow component of the velocity, $\sqrt{u^2 + v^2}$ (Fig. 1), becomes supersonic. The flow expands in going around the body, and the crossflow can become supersonic if the incidence is high enough. This component of velocity must be small in the lee symmetry plane due to the boundary conditions. A supersonic crossflow generally passes through a relatively normal shock before stagnating in the lee plane on the surface. The crossflow shock exists to turn the three-dimensional flow parallel to the lee symmetry plane. The variation in strength of the crossflow shock can be quite large. The shock is strongest at the body where the crossflow is highly supersonic and approaches zero strength in the field where the crossflow becomes sonic. It is this variation in strength that

produces a crossflow entropy gradient and thus radial vorticity. This vorticity in turn causes shock induced separation.

The low pressure side of the crossflow shock is computed with one-sided differences away from the shock. This is consistent with the fact that the crossflow is supersonic. The Rankine-Hugoniot conditions, together with the compatibility condition along a bicharacteristic reaching the shock on its high pressure side, supply enough information to compute the deviation of each shock point from a conical ray in addition to all the primitive variables on its high pressure side. The bicharacteristic used is the one in the plane containing the local normal to the shock and the marching direction. All shock points are computed with the post correction scheme proposed by Rudman¹⁷ and independently by deNeef¹⁸. The shocks converge (i.e., each shock point becomes aligned with a conical ray) with the rest of the flow field. In all the computations presented here, the last crossflow shock point fit had a normal Mach number of approximately 1.05 (pressure ratio of 1.12). The finite difference scheme was able to capture weaker shock points. In addition, the finite difference scheme was used to capture all reverse crossflow shocks and oblique crossflow shocks in the flow field (to be discussed later). These shocks are usually weak and the scheme can capture them accurately.

The computational grid used in this work is developed in stages. In the first stage, the elliptic cross section in a constant z plane is mapped to a circle. This step is omitted in the case of a circular cone. The mapping is a simple Joukowski transformation and will not be detailed here. Next, a polar coordinate system is used in the mapped space. An exponential stretching is used in the radial direction to cluster grid points near the surface in order to resolve the complex flow near separation. The Joukowski mapping, clusters grid points in the circumferential direction automatically. When thin ellipses (axis ratios > 10) were first considered, solutions with large truncation error at the wing leading edge were found. One result of this truncation error was the production of vorticity at the leading edge. There was little error in entropy at the leading edge (i.e., entropy was constant on streamlines), but the vorticity was large, leading to a violation of Crocco's theorem. The error was manifested by a layer in crossflow velocity at the surface. The crossflow on the body was much lower than that one point away from the body. While this vorticity was never large enough to

cause leading edge separation, as in the work of Ref. 9, 10, and 11, it did distort the separation behind the crossflow shock. This error was eliminated by increasing the resolution at the wing leading edge. An exponential stretching was used in the circumferential direction.

Shock induced inviscid separation produces a contact surface emanating from the separation point (Fig. 1). It is this contact that ultimately spirals to form a vortex. The contact surface has a jump in entropy and an accompanying jump in velocity. In conical flow, entropy is constant on crossflow streamlines. Thus, one can see (Fig. 1) that the entropy on the windward side of the contact comes from the windward stagnation point of a cone and the wing leading edge stagnation point in the case of an ellipse. The streamline that wets the body passes through the base of the crossflow shock to form the high entropy side of the contact. There are a number of possibilities for the entropy on the lee side of the contact. The crossflow streamlines that wet the body are tracked in each step of the iteration, and the proper entropy is imposed on the surface including the jump in entropy at the separation point. The entropy discontinuity off the body is captured with the finite difference scheme. The computation of the vortex sheet in the shed vorticity computation will be discussed in another section of this paper.

The finite difference scheme used in this work is an explicit marching scheme which is notoriously inefficient for converging to a conical or steady solution. One advantage of the explicit marching scheme is that it is totally "vectorizable." The time consuming parts of the code (i.e., interior point computation) utilized the vector architecture of the Cray 1 computer. This made the computation about 20 times faster than on an IBM 3033. The computations shown here typically took 45 CPU minutes on the Cray 1, and the grid used had 81 x 81 points in the cross sectional plane. In each case shown, the maximum residual (i.e., the derivative of pressure in the marching direction) was reduced at least six orders of magnitude.

3. COMPUTATIONAL RESULTS - SHOCK INDUCED VORTICITY

In this section, computational results showing spiralling streamlines due to the vorticity produced by a crossflow shock will be analyzed. The first configuration considered is a 10° half angle cone at $M_\infty = 2$ and $\alpha = 25^\circ$. The surface pressure distribution is shown in Fig. 2. This flow field has a shock induced separation at $\theta = 149.6^\circ$. In Fig. 2, the computed surface pressures using two grids are shown. Both computations 73×73 and 89×89 give the same separation point and spiral location, indicating an independence of the results to numerical viscosity due to truncation error. As a matter of fact, this flow field was computed with an even coarser grid (37×37) that exhibits the same basic features (i.e., separation and spiral).

The crossflow streamlines are shown in Fig. 3, along with the computed bow and crossflow shocks. The streamlines show saddles in the wind and lee symmetry planes on the cone surface. In addition, there is a saddle at the separation point and a node at the center of the spiral. The separation point and spiral can be seen more clearly in the blowup of Fig. 4. If the nodes and saddles are summed using the procedure of Ref. 4, it can be shown that the proper number of nodes and saddles exist in the streamline pattern of Fig. 3. The separation point ($\theta_s = 149.6^\circ$) corresponds to the plateau in pressure (Fig. 3) just after the shock. If one considers the momentum equation in the θ direction, it indicates that $\partial p / \partial \theta = 0$ at a crossflow stagnation point ($u = v = 0$). The separation point in this flow field is a real crossflow stagnation point (i.e., the crossflow passes continuously through zero). The streamlines (Fig. 4) show that the flow moves in the negative θ direction from the lee stagnation point toward the separation point. In doing so, the flow expands (i.e., there is a drop in pressure between $\theta = 180^\circ$ and $\theta = 165^\circ$). The flow then recompresses to the separation point. This recompression phenomenon is the cause of secondary separation. The inviscid separation point location is far from that of the viscous flow. This can be surmised by the fact that the shock is strong enough to separate a boundary layer at its base. The inviscid separation point is too far downstream of the shock. The streamlines of Fig. 4 clearly show how all the flow is ultimately swept up into the infinitely turning spiral. The apparent power of the Euler equations to describe the region near the center of the spiral should be noted. A

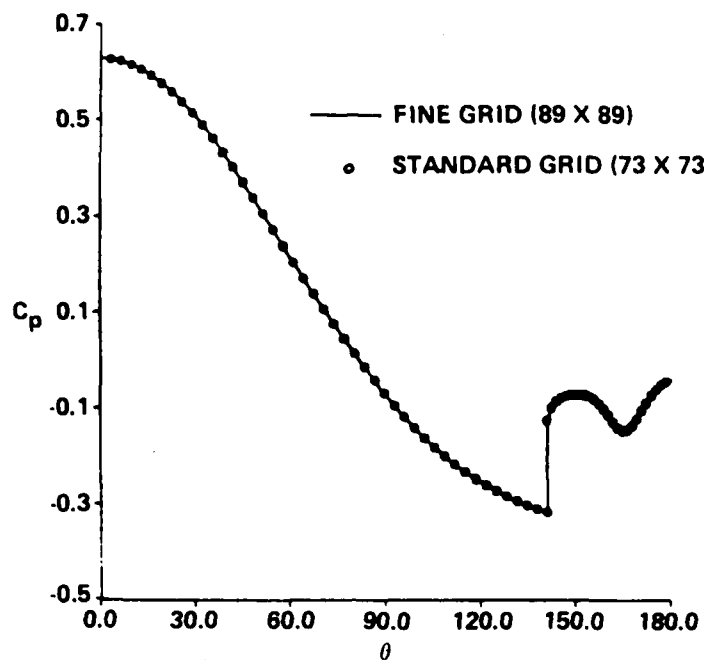


Fig. 2 Comparison of Computation with Two Grids,
Surface Pressure ($M_\infty = 2$, $\delta = 10^\circ$, $\alpha = 25^\circ$)

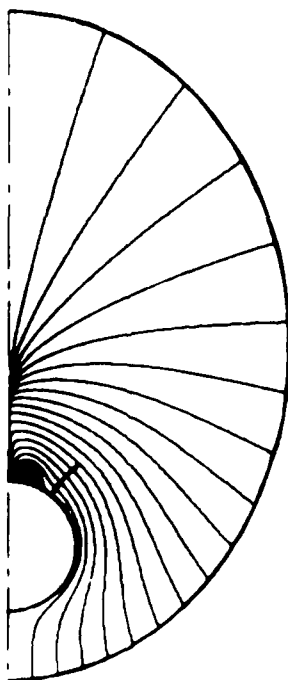


Fig. 3 Cross Flow Streamlines in Field ($M_\infty = 2$,
 $\delta = 10^\circ$, $\alpha = 25^\circ$)

detailed study of the streamline pattern near the center of the spiral revealed that the streamlines asymptote to an ellipse. This was first indicated by Smith (Ref. 5). It also should be pointed out that Fig. 4 shows that streamlines wrapping around the spiral very rapidly approach the lee side of the separation line (contact). Consider, for example, the third streamline off the cone in Fig. 4. It wraps around the top of the spiral, comes back and approaches the contact a short distance off the body, creating an entropy layer on the lee side of the contact. This entropy layer tends to weaken the contact.

Figure 4 also shows that the separation line leaves the cone at a finite angle. J.H.B. Smith's analysis (Ref. 5) concluded that at a forced separation the sheet comes off tangent. However, this difference is due to the fact that the separation in the shock induced case is highly nonisentropic. As such the flow can and does stagnate on both sides of the separating sheet. Figure 5 shows the crossflow velocity on the surface of the body ($v = 0$ from the body boundary condition). The point to be considered here is that the velocity passes through zero (separation) smoothly. The analysis of Smith indicates that separation occurs at a discontinuity in crossflow, the jump in velocity determining the sheet strength. This is a basic difference between forced and shock induced separation and is discussed in detail in Ref. 12. The jump in crossflow velocity in Fig. 5 is due to the shock. It is also interesting to note the maximum negative u that occurs under the spiral. This negative crossflow can become supersonic, causing a second reverse crossflow shock. A sample of this will be shown later.

Figure 6 shows the isobars for the same case ($M_\infty = 2$, $\delta = 10^\circ$, $\alpha = 25^\circ$). It should be noted how smoothly the crossflow shock transitions to zero strength in the field. The most interesting aspect of the figure is the closed isobar at the center of the spiral. It represents an absolute minimum in the flow field pressure. The component of vorticity in the spherical radial direction is given by:

$$\Omega_r = - (u \cos \phi + \frac{\partial u}{\partial \phi} \sin \phi - \frac{\partial v}{\partial \theta}) / (r \sin \phi)$$

where u and v are the crossflow velocities defined in Fig. 1 and r , θ , ϕ are spherical coordinates (Fig. 1). Figure 7 shows lines of constant $r\Omega_r$. The

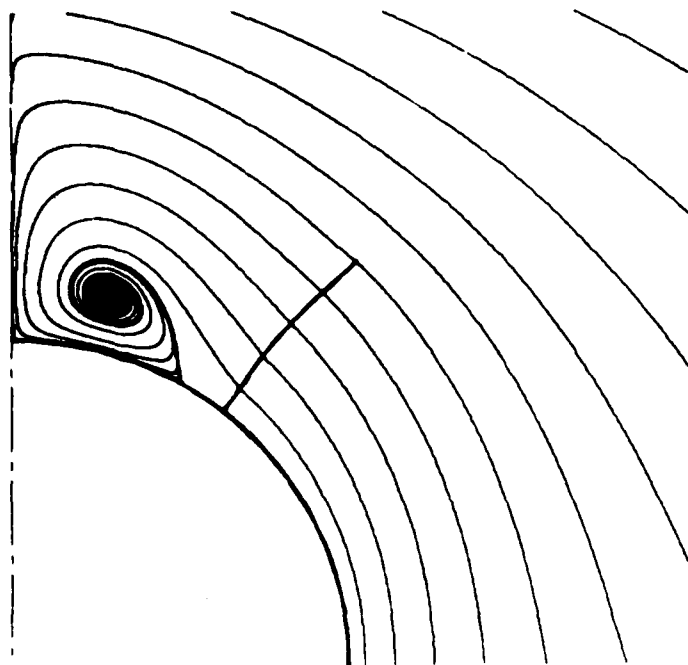


Fig. 4 Cross Flow Streamlines Near Lee Plane
($M_\infty = 2$, $\delta = 10^\circ$, $\alpha = 25^\circ$)

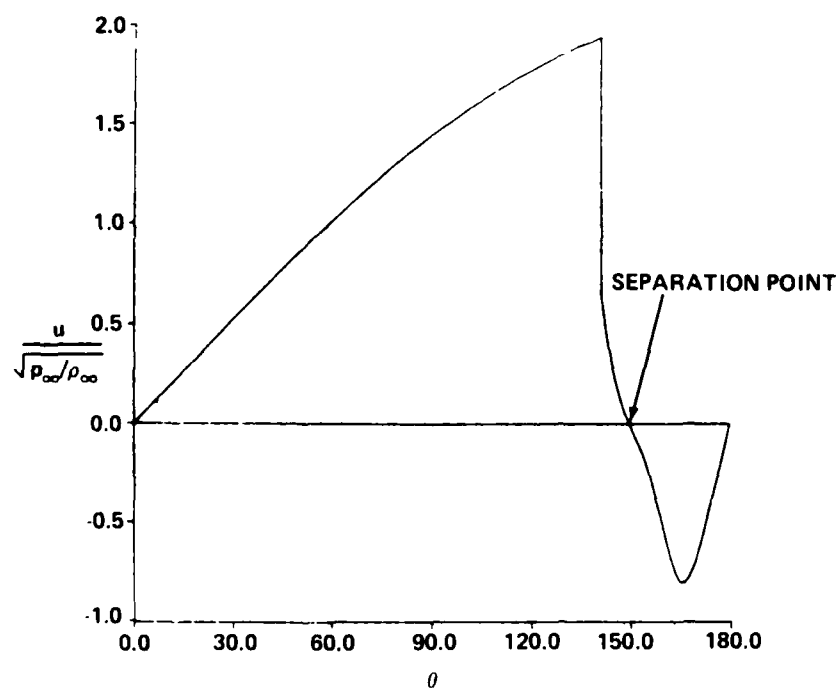


Fig. 5 Surface Cross Flow Velocity ($M_\infty = 2$,
 $\delta = 10^\circ$, $\alpha = 25^\circ$)

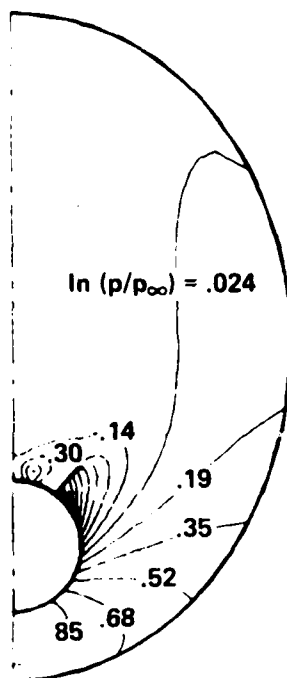


Fig. 6 Isobars in Cross Plane ($M_\infty = 2$, $\delta = 10^\circ$, $\alpha = 25^\circ$)

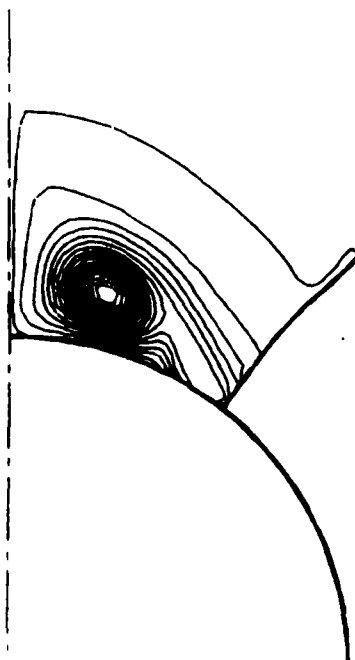


Fig. 7 Lines of Constant Radial Vorticity X Spherical Radius ($M_\infty = 2$, $\delta = 10^\circ$, $\alpha = 25^\circ$)

figure shows how the vorticity is distributed and is produced by the crossflow shock. Note that Ω_r is small until the crossflow shock, indicating that the bow shock doesn't produce enough vorticity to cause separation on its own. The vorticity produced by the bow shock is an order of magnitude smaller than that produced by the crossflow shock and two orders of magnitude smaller than that at the center of the spiral. For this reason, there are no contours of vorticity outside the region behind the crossflow shock in Fig. 7. The vorticity is negative, causing the counterclockwise spiraling of this flow, and its absolute magnitude is maximum at the center of the vortex.

The existence of a crossflow shock does not necessarily imply enough vorticity to cause separation. It is the variation in shock strength which produces an entropy gradient and thus vorticity which causes separation behind the shock. In the case of the circular cones considered thus far, the shock strength decreases monotonically from its base. This is not always the case, as will be discussed in the case of elliptic cross sections. For a circular cross section the shock strength at the surface is a good indication of the vorticity produced by the shock. Figure 8 is a plot of the inviscid separation point location vs the shock pressure ratio at the surface. The cone has a 10° half angle, and the free stream Mach number is 2. The crossflow shock strength was increased by increasing incidence. The pressure ratio used is a good measure of the shock strength variation and thus the vorticity produced by the shock. At each data point, the corresponding α is noted. The plot shows that as the shock strength decreases, the separation point moves to the lee symmetry plane. At the same time, the spiral region is getting smaller. The highest incidence computed was 25° , since above that value the axial Mach number on the cone surface approaches sonic, making it impossible to march. At the low end, $\alpha = 19^\circ$, the spiral was so small that it was difficult to resolve numerically, and no lower incidences are shown. The interesting feature of this figure is that an extrapolation of the curve would seem to indicate that inviscid separation moves to the lee plane before the shock is eliminated ($p_2/p_1 = 1$). An extrapolation would indicate that the spiral is eliminated at $p_2/p_1 \approx 1.85$. This corresponds to a normal Mach number slightly above 1.3, which is approximately the region where the full potential approximation is valid for these flow fields. It would seem that below a maximum normal Mach number of 1.3, the crossflow shock may not produce enough vorticity to cause separation.

Figures 9, 10 and 11 deal with an interesting case ($M_\infty = 3$, $\delta = 9.46^\circ$, and $\alpha = 25^\circ$). Figure 9 shows the streamlines and the crossflow shock near the lee plane. The shock exhibits a kink as it passes from the influence of the spiral. Near the cone, the shock must deflect the streamlines upward in order that they may pass over the spiral; beyond the top of the spiral, this is no longer true and the shock acts like a normal shock. The two regions are separated by the kink in the shock, and the shock slope in the crossflow plane had to be differenced away from this point. Another interesting feature of this flow is the fact that the expansion of the reverse flow from the lee stagnation point is so large that the negative crossflow becomes supersonic near the body. The smooth recompression shown in Fig. 2 is replaced by a reverse crossflow shock. This phenomenon has been noted experimentally in Ref. 19. The reverse crossflow shock, which was captured, can be seen in the isobars of Fig. 10. The second (reverse) shock is on the lee side of the primary crossflow shock. It is indicated by the clustering of the isobars between $\ln(p/p_\infty) = -1.2$ and $\ln(p/p_\infty) = -0.73$ on the cone surface. The shock is not strong enough to produce a secondary inviscid separation, whereas in the experiment of Ref. 19 it was strong enough to separate the boundary layer. The strength of the vortex is also indicated in Fig. 10 by the closed isobars representing a steep pressure minimum at the vortex center.

Figure 11 shows the surface pressure for the $M_\infty = 3$, $\delta = 9.46^\circ$ and $\alpha = 25^\circ$ case. The solid line is the present calculation with shock vorticity induced separation at $\theta = 155.3^\circ$, again at the plateau in pressure just after the primary crossflow shock. The reverse crossflow shock can be seen in the pressure distribution at about $\theta = 167^\circ$. The shock is captured, and so it is smeared over a mesh interval. The figure also shows the numerical results of Ref. 20. They are also a solution to Euler's equations but with the primary crossflow shock captured. In the results of Ref. 20, the separation point was forced to occur at $\theta = 120^\circ$ in order to match the boundary layer separation point found experimentally. The forced separation model of Ref. 20 is in contradiction to the analytical work of J.H.B. Smith (Ref. 5). In addition, there are anomalies in the results of Ref. 20. Basically the comparison of Fig. 11 shows that the two results are very close, while the separation points are very different. It seems that forcing separation at $\theta = 120^\circ$ simply inserted a wiggle in the surface pressure distribution of Ref. 20. The flow then came back to the shock induced flow field. The crossflow shock locations

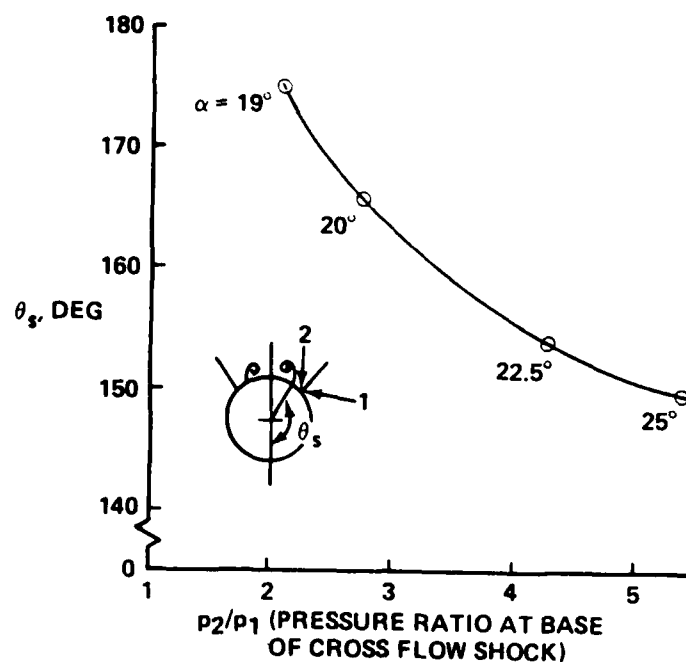


Fig. 8 Inviscid Shock Induced Separation Point Location vs Shock Strength ($M_\infty = 2$, $\delta = 10^\circ$)

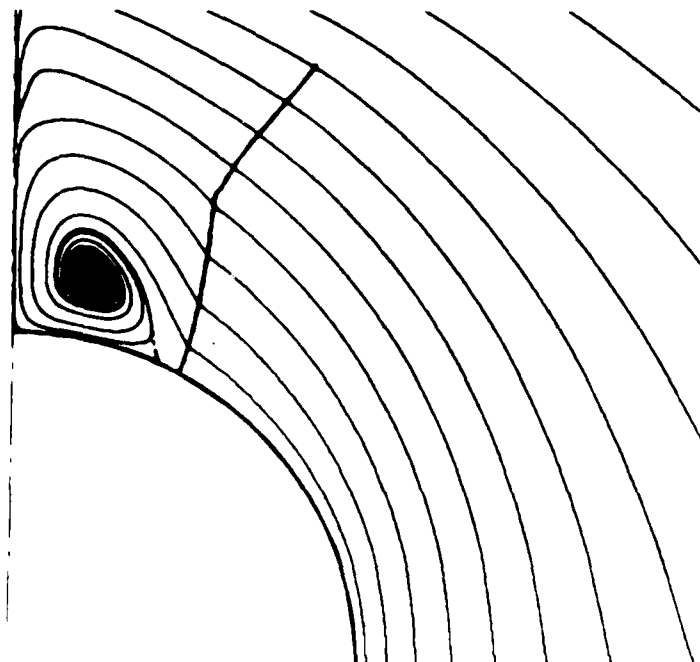


Fig. 9 Cross Flow Streamlines Near Lee Plane ($M_\infty = 3$, $\delta = 9.46^\circ$, $\alpha = 25^\circ$)

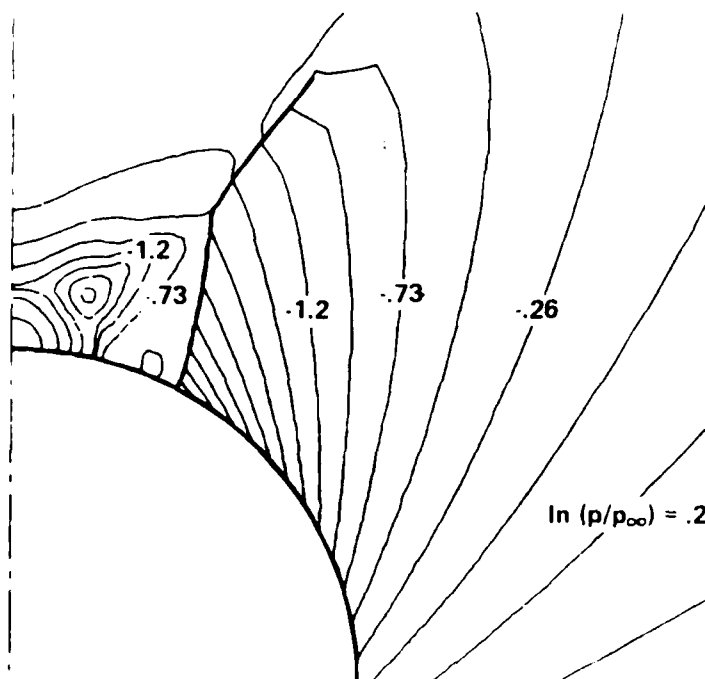


Fig. 10 Isobars Near Lee Plane ($M_\infty = 3$, $\delta = 9.46^\circ$, $\alpha = 25^\circ$)

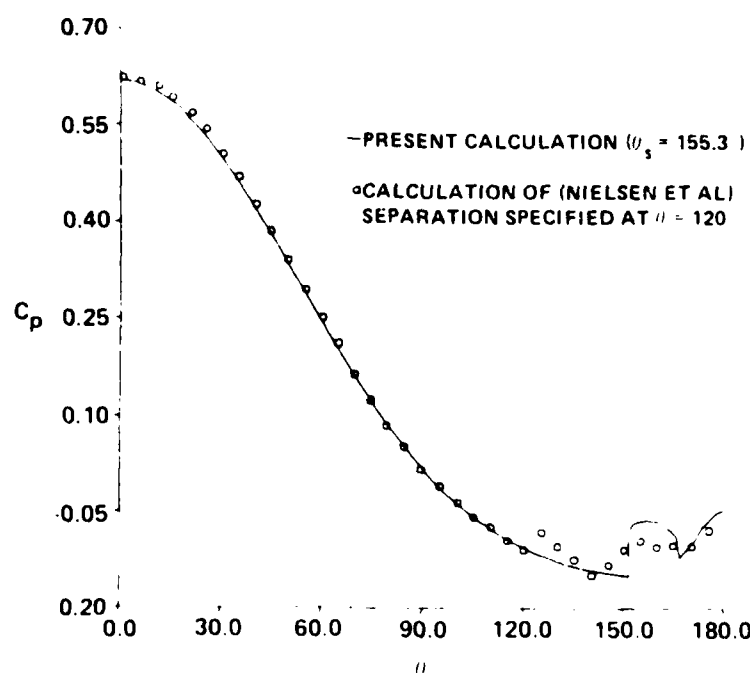


Fig. 11 Surface Pressure Comparison ($M_\infty = 3$, $\delta = 9.46^\circ$, $\alpha = 25^\circ$)

are very close. The shock of Ref. 20 is smeared over a few points but is close to the fit shock of the present calculations. If separation did occur at 120° , there must be a crossflow shock before $\theta = 120^\circ$. However, there is no evidence of a shock before separation in the results of Ref. 20.

Figure 12 shows the pressure distribution on a 5° cone at $M_\infty = 4.25$ and $\alpha = 12.35^\circ$. Compared are the results of the present calculation, those computed using the full potential equation supplied by M. Siclari²¹, and the experimental results of Rainbird²². The potential results of Siclari have been corrected for nonisentropic bow shock effects while maintaining the irrotational assumption. Figure 12 indicates that the Euler and potential results are virtually identical until the shock. The potential result does not exhibit the minimum in pressure behind the shock typical of separation. Potential calculations cannot predict separation or spiraling without a shedding sheet. The comparison between the Euler and potential calculations affirms the fact that rotationality is important only after the crossflow shock. A comparison between the present calculation and the experimental results of Rainbird clearly shows that the vorticity produced by the shock does not separate the flow near the viscous separation point. The experimental data show two separations, primary at $\theta = 120.3^\circ$ and secondary at 160° , while the inviscid separation is at $\theta = 151.3^\circ$. The longer plateau in pressure in the experiment behind the primary separation point is due to the secondary separation; otherwise, the Euler and experimental pressure distributions would be similar. It is the expansion and recompression of the reverse flow that causes secondary separation. It should be clear that while the vorticity produced by the crossflow shock is not the whole separation story, it may play an important role in the process. There are two sources of vorticity in this flow field: one is the shock and the other the boundary layer. Both these sources of vorticity play a role in separation and the resulting spiral or vortex. Boundary layer shed vorticity will be discussed later in this paper.

The eccentricity of the elliptic cross sections has a significant impact on the vorticity generated by the crossflow shock. In general, the thinner the cross section (higher axis ratio) the stronger the shock. There is an effect, discovered by the author¹³, which seems to reduce the entropy gradient near the surface behind the shock as the section of elliptic delta wings gets

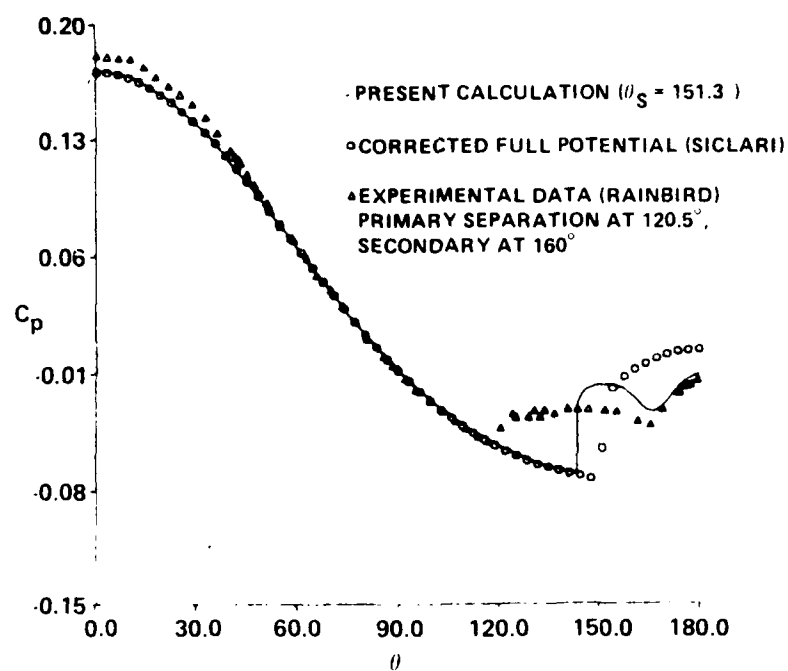


Fig. 12 Surface Pressure Comparison ($M_\infty = 4.25$,
 $\delta = 5^\circ$, $\alpha = 12.35^\circ$)

thinner. Consider the isobar plots of Fig. 13 and 14; both show the leading edge of the wing, crossflow shock and isobars in the leading edge region. Figure 13 shows a 10:1 section and Fig. 14 a 6:1 section. The other parameters of the flow were chosen so that the shock was approximately the same strength at the surface. The two angles noted in the figure define the wing geometry, λ is the sweep angle of the delta, and δ is the slope of the surface in the symmetry plane. In the thinner case (Fig. 13), there is a gap between the surface and the last wave of the expansion from the wing leading edge. This is indicated by the tendency of the isobars to become more vertical near the shock. The effect is similar to the uniform flow region downstream of a Prandtl-Meyer expansion below the last wave of the expansion. The result of this phenomenon is a region of uniform crossflow Mach number in front of the shock near the surface. This region is indicated in Fig. 13 by the portion of the shock near the surface before it begins to curve. An inspection of Fig. 14 shows that this effect is not present because the leading edge radius of curvature is too large in this case.

The result of this phenomenon is shown in Fig. 15, which is a plot of the entropy distribution along the shock on its high pressure side. Note the much smaller entropy gradient in the 10:1 case as compared with the 6:1 case. Also included in the figure is the entropy distribution along the crossflow shock for the 10° cone, $M_\infty = 2$, and $\alpha = 25^\circ$ discussed previously. Although the shock is much stronger for the case of the cone, this curve is included for reference. Note that the entropy drops rapidly at the surface in the case of the cone. The vorticity just behind the shock at the surface is much larger in the 6:1 case than in the 10:1 case. The result is that the 6:1 case separates and the 10:1 does not. Figure 16 shows the crossflow Mach number distribution on the surface for the three cases. First note that the 6:1 and 10:1 cases have the same shock strengths as were indicated by their surface entropies at the shock (Fig. 15). The separation in the 6:1 case is indicated by the negative Mach number starting at $\bar{\theta} \approx 160^\circ$ ($\bar{\theta}$ is the polar angle in the mapped space). While it is true that increasing the eccentricity of the section tends to decrease the entropy gradient behind the shock, this does not always eliminate separation. The vorticity just behind the shock at the wall may be reduced, but it can become large downstream and cause separation. In addition, once a spiral forms, the shock has a tendency to move toward the

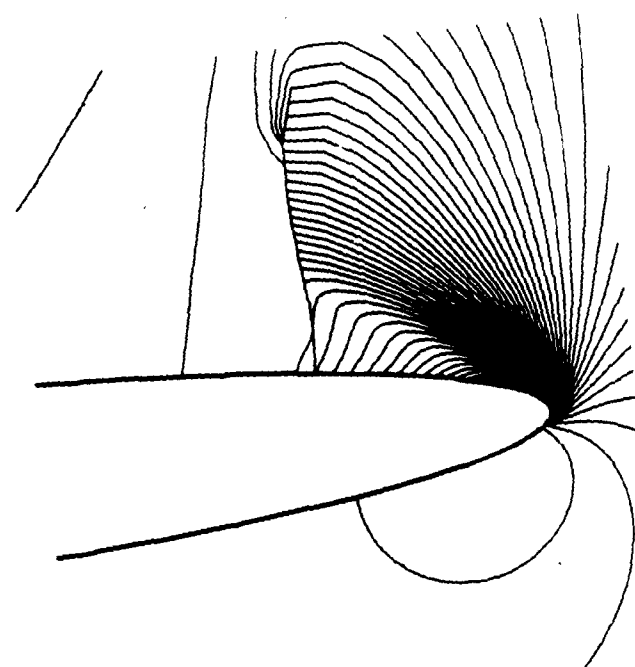


Fig. 13 Isobars Near Leading Edge & Shock ($M_\infty = 2$,
 $\alpha = 10^\circ$, Ellipse, $\delta = 2.08^\circ$, $\lambda = 70^\circ$)

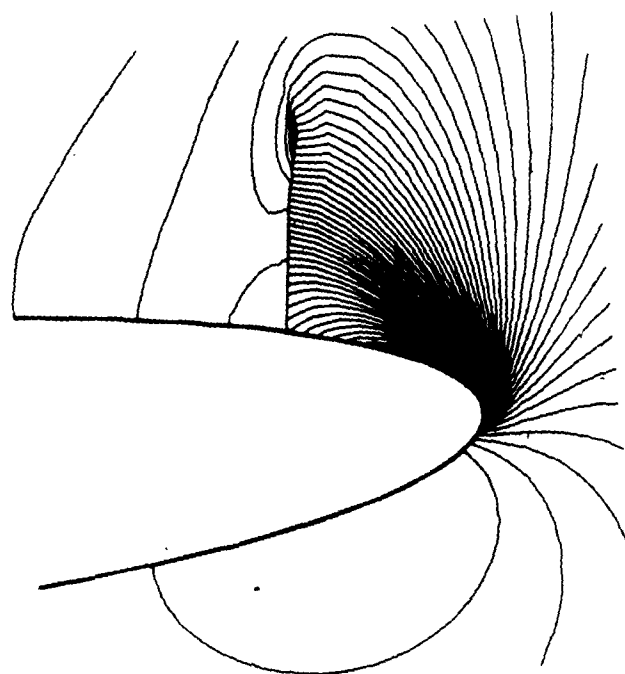


Fig. 14 Isobars Near Leading Edge & Shock ($M_\infty = 1.97$,
 $\alpha = 10^\circ$, 6:1 Ellipse, $\delta = 3.17^\circ$, $\lambda = 71.61^\circ$)

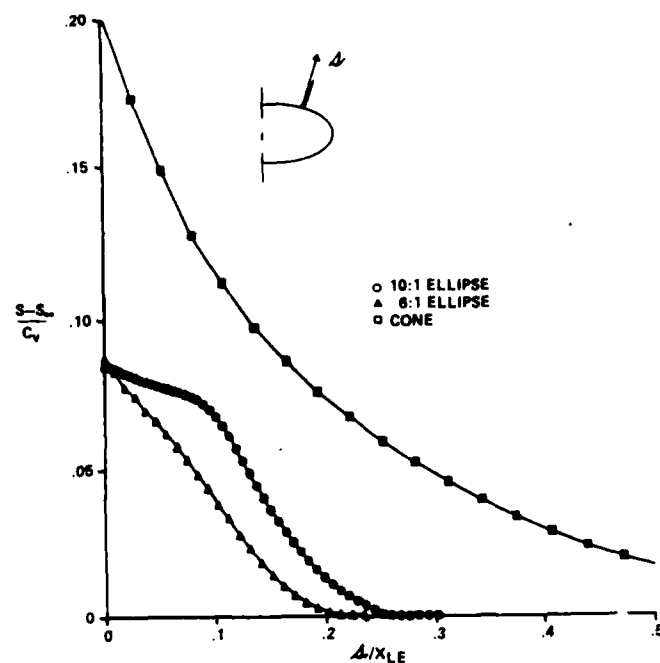


Fig. 15 Entropy Distribution Along the Shock
 (10:1 Ellipse, $M_\infty = 2$, $\alpha = 10^\circ$, $\delta = 2.08^\circ$, $\lambda = 70^\circ$) (6:1 Ellipse, $M_\infty = 1.97$, $\alpha = 10^\circ$, $\delta = 3.17^\circ$, $\lambda = 71.61^\circ$)
 (Cone, $M_\infty = 2$, $\alpha = 25^\circ$, $\delta = 10^\circ$)

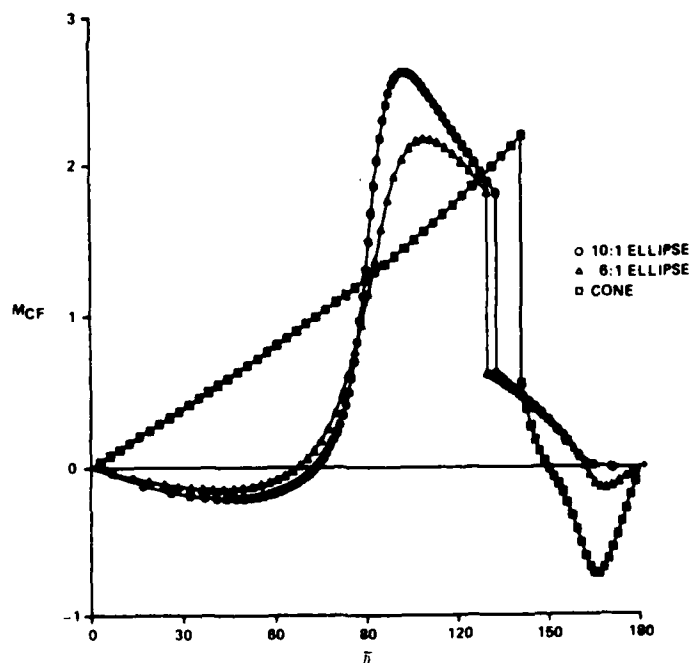


Fig. 16 Surface Crossflow Mach Number Distribution
 (10:1 Ellipse, $M_\infty = 2$, $\alpha = 10^\circ$, $\delta = 2.08^\circ$, $\lambda = 70^\circ$) (6:1 Ellipse, $M_\infty = 1.97$, $\alpha = 10^\circ$, $\delta = 3.17^\circ$, $\lambda = 71.61^\circ$) (Cone, $M_\infty = 2$, $\alpha = 25^\circ$, $\delta = 10^\circ$)

leading edge where the extent of the uniform flow region just discussed is reduced. The problem is complicated by a number of factors.

The next case considered is a very thin delta wing. The ellipse axis ratio is 14:1 ($\delta = 1.5$, $\lambda = 70^\circ$); the freestream conditions are $M_\infty = 2$ and $\alpha = 10^\circ$. The crossflow shock is somewhat stronger in this case than the ellipse discussed in the last paragraph. The shock crossflow Mach number at the surface is 1.9 in this case and was about 1.8 in both the 6:1 and 10:1 cases discussed previously. This is due to the higher eccentricity. The eccentricity of this section combined with a shock position relatively far from the leading edge results in a significant region of uniform flow near the base of the shock. This is indicated by the isobar plot of Fig. 17. The result is a very small derivative of entropy normal to the surface just behind the shock. The flow in this case does separate although the effect is mild. It seems that the eccentricity of the section has reduced the vorticity resulting in a weak vortex. Figure 18 shows the surface pressure distribution for this case compared with the computed results of R. Newsome.¹¹ The effect of the vortex is seen as a slight drop in the upper surface pressure, the local minimum is at about $X/X_{LE} = 0.3$. The influence of the separation is negligible in this case, as demonstrated in the next paragraph. The comparison is very good, although the influence of the vortex in the result of Ref. 11 seems a little greater. In the work of Newsome, the shock was captured and is spread over four mesh intervals. This is good in light of the fact that no post or preshock overshoots are present. It seems that these are controlled with artificial damping (see Ref. 11 for details). No such damping was necessary in the present calculation because the shock is fit. It is interesting that the artificial damping can be controlled so that the shock vorticity induced separation is not distorted significantly.

In an effort to study a substantial shock vorticity induced vortex on a delta wing, a flow situation was developed in which the crossflow shock strength at the surface was large. It was shown by Siclari²³ that for potential flows, the shock strength is increased as the wing leading edge sweep is increased. A 10:1 ellipse whose leading edge was swept 72° (i.e., $\lambda = 72^\circ$ and $\delta = 1.86^\circ$) was considered. The freestream conditions were the same as those considered previously ($M_\infty = 2$, $\alpha = 10^\circ$). The surface shock Mach number was 2.3 in this case while it was only 1.8 for the 10:1 ellipse

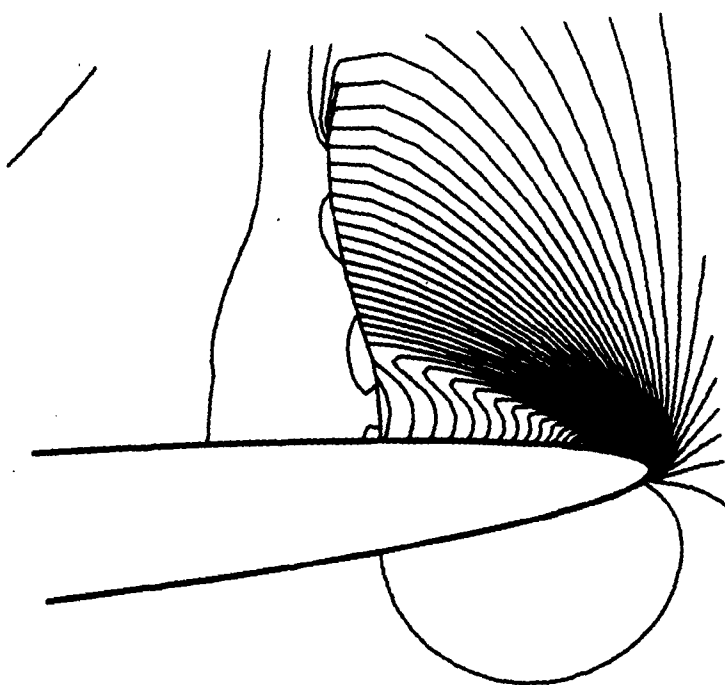


Fig. 17 Isobars Near Leading Edge & Shock ($M_\infty = 2$, $\alpha = 10^\circ$, 14:1 Ellipse, $\delta = 1.5^\circ$, $\lambda = 70^\circ$)

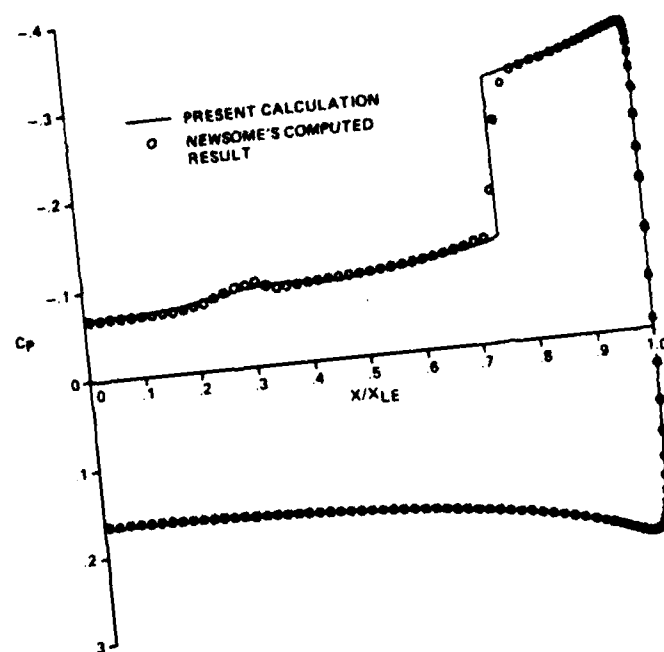


Fig. 18 Surface Pressure Comparison ($M_\infty = 2$, $\alpha = 10^\circ$, 14:1 Ellipse, $\delta = 1.5^\circ$, $\lambda = 70^\circ$)

considered previously. The flow did separate in this case, and the vortex was substantial (maximum reverse Mach number of -0.78). The crossflow streamlines are shown in Fig. 19. The dashed line that intersects the body near the leading edge (the stagnation point is a saddle) is the streamline which wets the surface. The entropy on this crossflow streamline wets the surface from the saddle to the wind plane node, and over the leading edge through the shock and separates onto the spiralling contact sheet. The dashed line that attaches to the surface near the lee plane carries the entropy which wets the surface from its saddle to the lee plane node and back in the reverse flow region to the low entropy side of separating contact. Figure 20 shows the region near the leading edge in more detail. The figure shows the crossflow shock whose shape is affected by the vortex. The dashed line near the vortex is the separating streamline, i.e., the contact sheet.

Figure 21 shows the isobar pattern (for the case discussed in the last paragraph) near the leading edge. Note that the separation has moved the shock toward the leading edge so that the region of uniform flow near the base of the shock does not exist in this case. The entropy gradient behind the shock is quite large so that the vorticity generated by the shock is significant. The closed isobar downstream of the shock represents a minimum in pressure which corresponds to the center of the vortex. The effect of the separation on all aspects of the flow field is significant. In particular, the surface pressure is affected significantly. Figure 22 compares the computed surface pressure with that calculated using the full potential equation. Again the two calculations give the same result up to the location of the shock. The shock position is moved from $X/X_{LE} \approx 0.73$ (potential) to $X/X_{LE} \approx 0.83$ (Euler) by the separation. In addition, all the typical separated flow features behind the shock do not exist in the potential result. The maximum in pressure just behind the shock represents the separation or stagnation point and the minimum in pressure at $X/X_{LE} \approx 0.6$ represents the maximum in reverse flow velocity just under the vortex.

The results shown thus far have indicated that shock vorticity can cause separation which is at least qualitatively similar to boundary layer separation. In addition, the computations have shown that shock vorticity can have a significant impact on the flow field. The rest of this paper will deal with the impact of vorticity shed from a separating boundary layer.

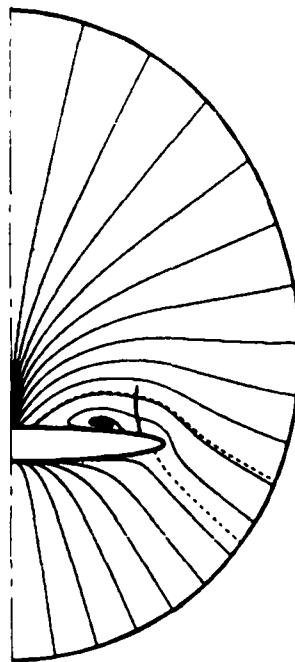


Fig. 19 Crossflow Streamlines ($M_\infty = 2$,
 $\alpha = 10^\circ$, 10:1 Ellipse, $\delta = 1.86^\circ$,
 $\lambda = 72^\circ$)



Fig. 20 Crossflow Streamlines Near Leading Edge ($M_\infty = 2$,
 $\alpha = 10^\circ$, 10:1 Ellipse, $\delta = 1.86^\circ$, $\lambda = 72^\circ$)

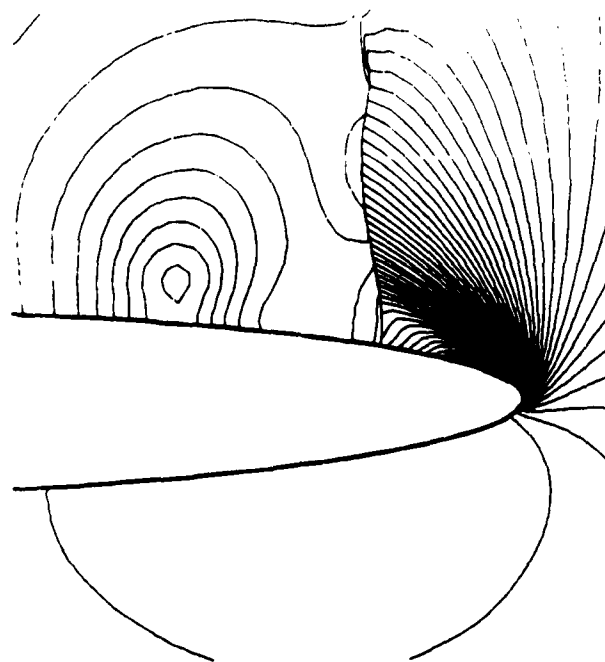


Fig. 21 Isobars Near Leading Edge ($M_\infty = 2$, $\alpha = 10^\circ$, 10:1 Ellipse, $\delta = 1.86^\circ$, $\lambda = 72^\circ$)

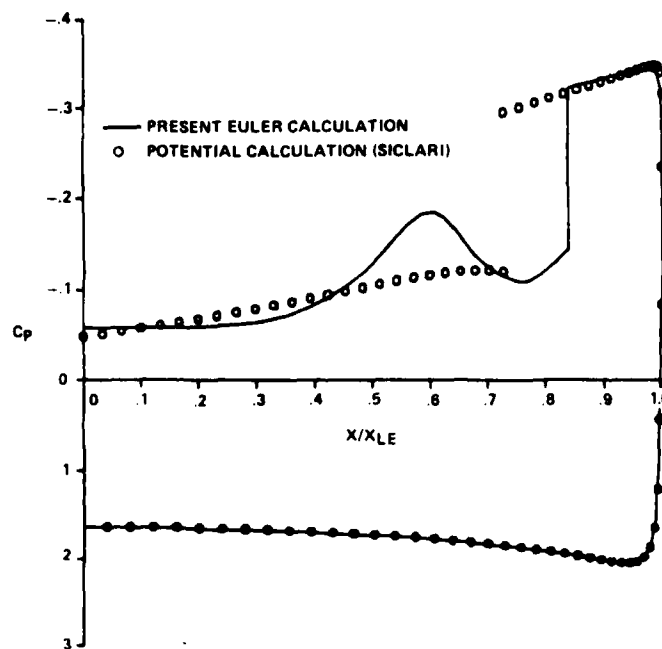


Fig. 22 Surface Pressure Comparison ($M_\infty = 2$, $\alpha = 10^\circ$, 10:1 Ellipse, $\delta = 1.86^\circ$, $\lambda = 72^\circ$)

4. SHED VORTICITY - COMPUTATIONAL MODEL

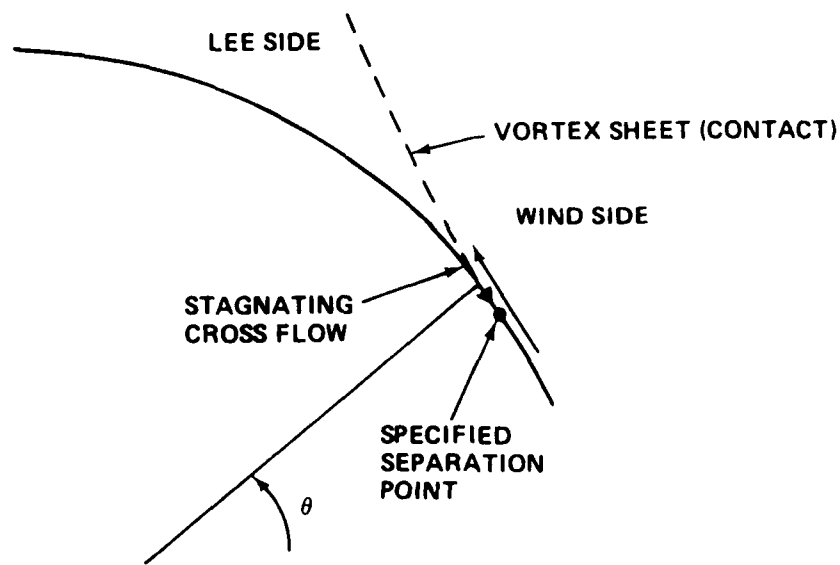
In this section, the concept of shedding vorticity from a specified separation point (the intersection of a conical separation line and the cross plane) will be discussed. The conceptual process of shedding vorticity from a conical surface will force separation and an accompanying spiral. The model used here to force separation at a specified location follows the work of J.H.B. Smith⁵. Smith assumed irrotational flow outside a vortex sheet in order to analyze the local flow at separation. The present work uses only the basic concept, which doesn't depend on the irrotational assumption. In addition, any model of inviscid separation should reduce to that of Smith as the rotationality outside the vortex sheet gets small. The basic concept acquired from Ref. 5 is that at a specified separation point, there is a vortex sheet or contact surface which has a jump in velocity direction. The condition at the intersection of the sheet and the surface (i.e., the separation point) is that the crossflow velocity stagnates on the lee side of the sheet (Fig. 23a). The crossflow velocity on the wind side of the sheet is determined by the global solution. In general, the crossflow velocity on the wind side of the sheet is finite. The vortex sheet is a stream surface and the pressure is continuous across it. In the case of isentropic irrotational flow considered in Ref. 5, these conditions imply that the modulus of velocity is continuous across the sheet. If the crossflow stagnates on both sides of the sheet ($u = v = 0$) at separation, the isentropic condition implies that the radial component of velocity (w , Fig. 1) is continuous and the sheet doesn't exist (i.e., no vorticity is shed into the flow field). These arguments conclude that in isentropic flow, the separating sheet must leave the cone surface tangentially if the wing side crossflow is subsonic. If the surface crossflow is subsonic just upstream of separation and the sheet leaves the surface at any angle relative to the surface, then the flow on the wind side of the sheet must stagnate and no vorticity will be shed into the flow. On the other hand, if the crossflow is supersonic the sheet can leave the surface at an angle, an oblique crossflow shock will occur, and the flow on the wind side of sheet will not stagnate so that vorticity is shed. This phenomenon will be discussed further in the next section. None of these arguments hold for the highly nonisentropic flow discussed in the previous section, where the flow

stagnates on both sides of the separating sheet. In these cases vorticity is not shed from the surface, only shock vorticity is present.

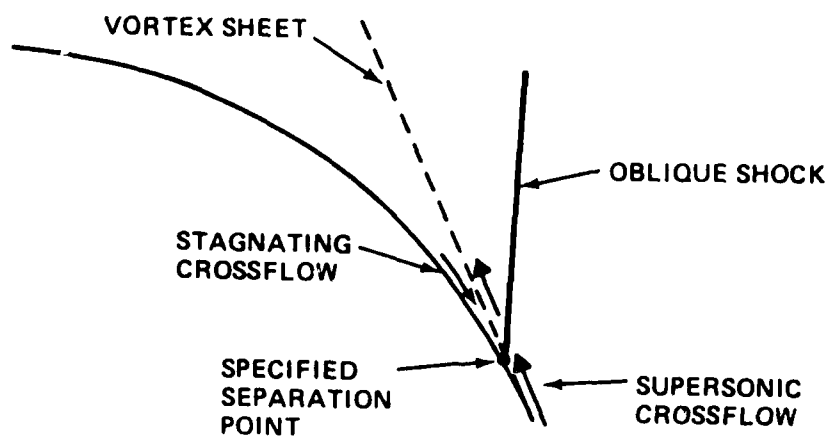
Separation was forced in the calculations presented here simply by using a double point at separation in order to allow for a jump in crossflow velocity. The crossflow velocity (u) on the wind side of the sheet is determined by the governing crossflow momentum equation, as at any other surface point. The crossflow component v must vanish at every surface point from the boundary condition. The crossflow velocity on the lee side of the sheet is set to zero ($u = 0$) in order to force separation at a specified point.

The separation point in this forced separation model exhibits a jump in crossflow velocity. The crossflow on the wind side (Fig. 23a) of the separation is evaluated in each step of the iteration from the momentum equation tangent to the body in the cross plane. The remaining primitive variables are computed at this point with the same governing equations as at any other body point, with the boundary condition ($v = 0$) satisfied. All circumferential velocity derivatives are taken one-sided in the negative θ direction in order to avoid differencing across the sheet. The point just below the sheet (lee side) is forced to be a crossflow stagnation point ($u = v = 0$). The pressure is continuous across the sheet so that its value on the wind side could theoretically be used on the lee side at separation. Difficulties were encountered in computing the pressure in a small region just after separation. The computation of the pressure in this region will be discussed in the next paragraph. The entropy at the lee side point is computed in the standard way (i.e., conserved along the streamline that wets the lee side of the body). If the pressure is known in addition to the entropy and total temperature (the flow is assumed adiabatic), the last component of velocity w (Fig. 1) can be evaluated from the energy equation. Again circumferential derivatives of the velocities across the sheet at the body grid points near separation are avoided. Differences in entropy across the sheet are avoided naturally by the λ -scheme as in the shock induced separation discussed in the previous section.

The difficulty encountered in the evaluation of the pressure on the lee side of the separation point can be traced to the numerical computation of the derivatives of velocities in a direction normal to the surface. The



a) Subcritical



b) Supercritical

Fig. 23 Sketch of Forced Separation Model

derivatives appear in the continuity equation from which the pressure is evaluated. These velocities are discontinuous across the sheet, and since the sheet lies so close to the surface at separation, there is no way to resolve the flow in the region between the surface and the sheet near separation. The behavior of the pressure in this region was evaluated analytically by Smith⁵ and numerically by Fiddes⁶ under the assumption of slender body theory. The results of Fiddes show a pressure plateau on the surface just after separation. The full Euler equations predict that the pressure derivative along the surface (p_θ) becomes zero at the lee side of the separation point, where the crossflow stagnates. In the present calculation it has been difficult to obtain this type of pressure behavior. A number of procedures have been attempted with varying degrees of success, but none has been totally satisfactory. In Ref. 7 the author showed preliminary results which exhibited a pressure plateau after separation, but the scheme used there proved unstable when the vortex sheet was moved during the iteration process. A reformulation of dependent variables has alleviated the problem. Currently, as long as the crossflow is subsonic (Fig. 23a) just before separation, no special treatment is used in evaluating the pressure except for circumferential and radial grid clusterings. Because of the difficulties associated with the pressure evaluation in the region on the surface just after separation the results of the next section should be considered somewhat preliminary.

In the case of supersonic crossflow (Fig. 23b) differencing of pressure across the separation point proved to be unstable. The results of a number of numerical experiments indicate that the model for the inviscid flow in this case should be such that the sheet leaves the surface at an angle relative to it, and an associated shock occurs at separation. The flow structure is sketched in Fig. 23b. This model does not violate the concepts of vorticity shedding proposed by Smith⁵ since the flow on the wind side of the separation point need not stagnate and thus a jump in velocity does exist across the sheet. In order to capture the shock at separation in one mesh interval no pressure derivatives were taken across the separation point on the cone surface. In addition a small pressure plateau is imposed just after separation, the level being taken from just downstream of separation.

It should be pointed out that the discussion presented in this section thus far has assumed a circular cross section. The velocity u is tangent to the body and v is normal. For an elliptic cone the procedure is the same with

u and v being replaced in the discussion by conical velocities tangent and normal to the body.

Secondary separation is forced by shedding vorticity from the body in the reverse crossflow region produced by primary separation. The model is the same as was just outlined for primary separation. Both separation point locations are obtained from experimental data. The only free parameters in the problem as posed here are the locations of the separation points. In the work of Ref. 6 primary separation points were found iteratively by matching an inviscid solution (slender body theory) to a boundary layer solution. A full viscid/inviscid interaction procedure using the current Euler calculation will be the subject of future work.

5. COMPUTATIONAL RESULTS - SHED VORTICITY

The procedure for shedding vorticity in an inviscid flow was tested by comparisons with the experimental data of Rainbird²². A 5° half angle cone was tested at $M_\infty = 1.79$ ($Re = 34 \times 10^6$) and $M_\infty = 4.25$ ($Re = 68 \times 10^6$). The detailed surface pressure distributions presented in Ref. 22 were digitized for comparison. Both primary and secondary separation point locations were determined from surface shear stresses in the measurements and used in the Euler computations. In addition, pitot pressure surveys were taken in the vicinity of separation, which were used to compare the experimental and computed vortex core locations. All the computations which follow were performed on an 89 x 89 cross sectional grid with residuals reduced at least five orders of magnitude.

The first case considered is the 5° cone at $M_\infty = 1.79$ and $\alpha = 12.65^\circ$. The crossflow is subsonic in this case and primary separation occurred at $\theta = 132^\circ$. Figure 24 shows the computed crossflow streamline pattern in the vicinity of separation. The vortex is clearly shown above the cone surface in Fig. 24. The dashed line leaving the surface tangentially is the vortex sheet. The dashed line off the surface is the crossflow streamline which stagnates at a saddle in the lee plane and partitions the flow which goes into a node in the lee plane (not shown in Fig. 24) from that which goes into the spiral node at the center of the vortex. The vortex center location compares reasonably well with that found experimentally. The experiment shows the location at $\theta = 165^\circ$ and $h = 0.2$ (h is the radial distance from the surface normalized by the cone radius) and the computation predicts the vortex location at $\theta = 162^\circ$ and $h = 0.18$. All the streamlines are well behaved including the separating streamline and those which spiral into the vortex. The power of the Euler equations to capture the flow features once vorticity is shed from the surface is clear from Fig. 24. Potential methods, linearized or fully nonlinear, require the inclusion of discrete vortices to model the sheet. This requirement usually precludes a description of the entire sheet, only a portion of the sheet is computed with the remainder being lumped into a single vortex. The only special treatment in the present work is that of shedding vorticity from one point on the surface as described in the last section.

Figure 25 shows the streamlines for the same case with both primary and secondary separation included. Secondary separation was imposed at $\theta = 156^\circ$ (from the data of Ref. 22) and is indicated by the lifting off of the surface streamline in the reverse flow region. The secondary vortex was too small to resolve with the grid used. Figure 26 shows the surface crossflow velocity distribution for this case, the reversals in velocity at the two separation points can be seen clearly. The inclusion of secondary separation affects the flow behavior substantially, in particular the location of the primary vortex and the surface pressure distribution. Unfortunately, it moves the vortex center to $\theta = 165^\circ$ and $h = 0.14$. With secondary separation included the computed radial location of the vortex center is further from the experimental data than with primary separation alone. It is obvious from the pitot pressure survey of Ref. 22 that secondary separation occurs in a region which has stronger viscous effects than primary separation. It may be that the prediction of flows with secondary separation with a purely inviscid model is impossible. The possibility that the computational difficulties in computing the flow in the region just after separation is affecting these results also exists.

The surface crossflow velocity distribution shown in Fig. 26 should be compared with that of Fig. 5 which only included shock vorticity. Figure 26 shows a discontinuity at primary separation from $u \approx .6$ to $u = 0$ and at secondary separation from $u \approx -.5$ to $u = 0$. Of course, it is these jumps in velocity which determine the vorticity which is shed from the separation points. In Fig. 5 the velocity passes through zero smoothly so that no vorticity is shed from the surface and only shock vorticity exists.

Figure 27 shows the surface pressure distribution computed assuming no separation, only primary separation and both primary and secondary separation also included are the experimental results. Primary separation occurs in the middle of the adverse pressure gradient of the attached flow ($\theta = 132^\circ$). Primary separation forces the flow to compress more rapidly upstream of separation which is consistent with the findings of Ref. 6 and the experimental data. In addition a reverse flow region is developed behind the separation point. This reverse flow expands from the lee plane to a local pressure minimum just under the vortex ($\theta \approx 162^\circ$) and recompresses to somewhat of a plateau (beginning at $\theta \approx 150^\circ$). This region exhibits

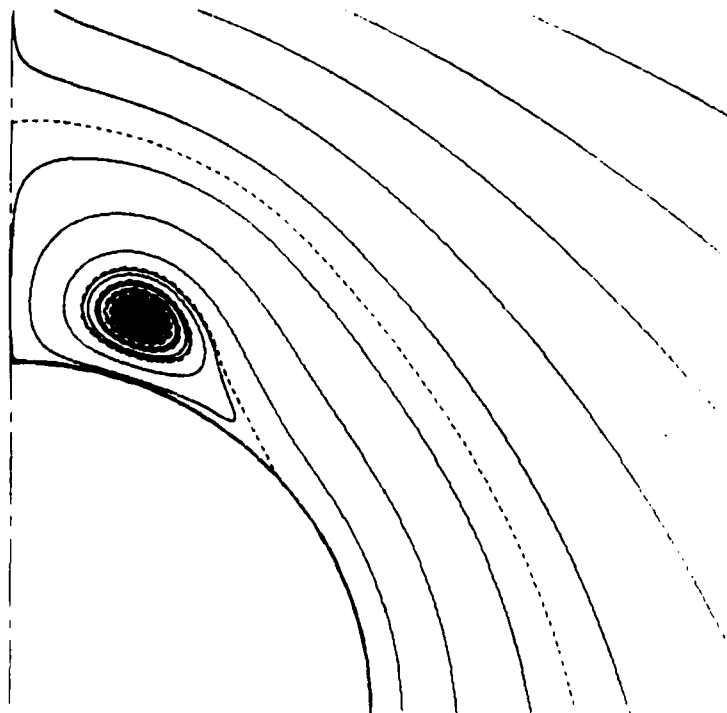


Fig. 24 Cross Flow Streamlines, Primary Separation
 ($M_\infty = 1.79$, $\delta = 5^\circ$, $\alpha = 12.65^\circ$)

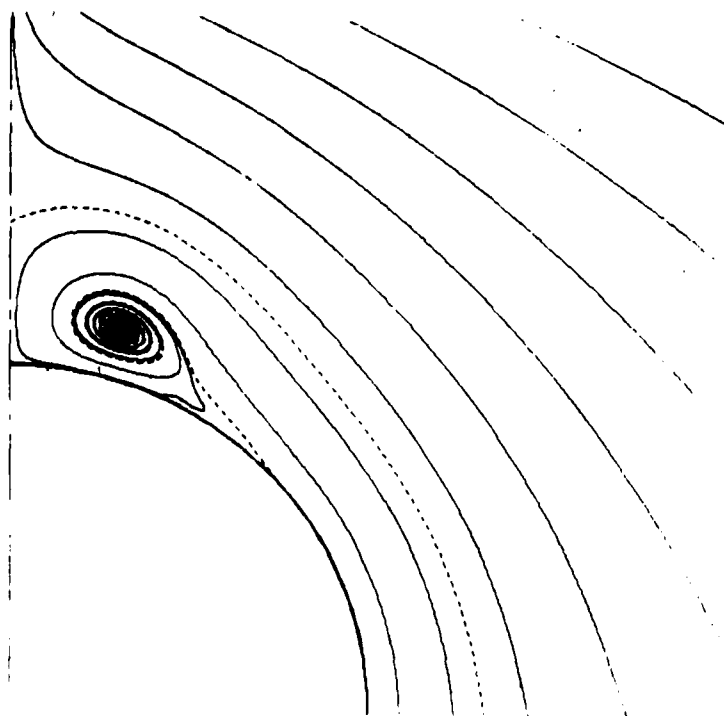


Fig. 25 Cross Flow Streamlines, Primary & Secondary
 Separations ($M_\infty = 1.79$, $\delta = 5^\circ$, $\alpha = 12.65^\circ$)

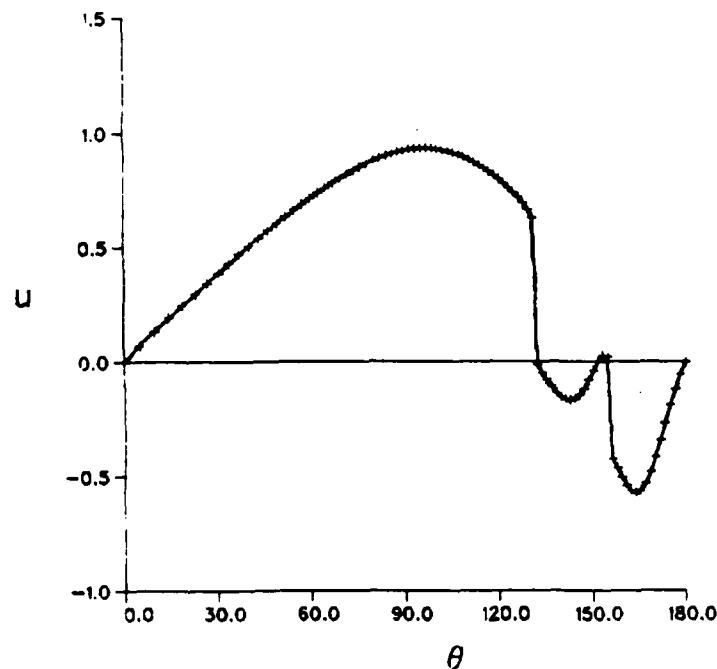


Fig. 26 Surface Crossflow Velocity Distribution,
Primary and Secondary Separations
($M_\infty = 1.79$, $\delta = 5^\circ$, $\alpha = 12.65^\circ$)

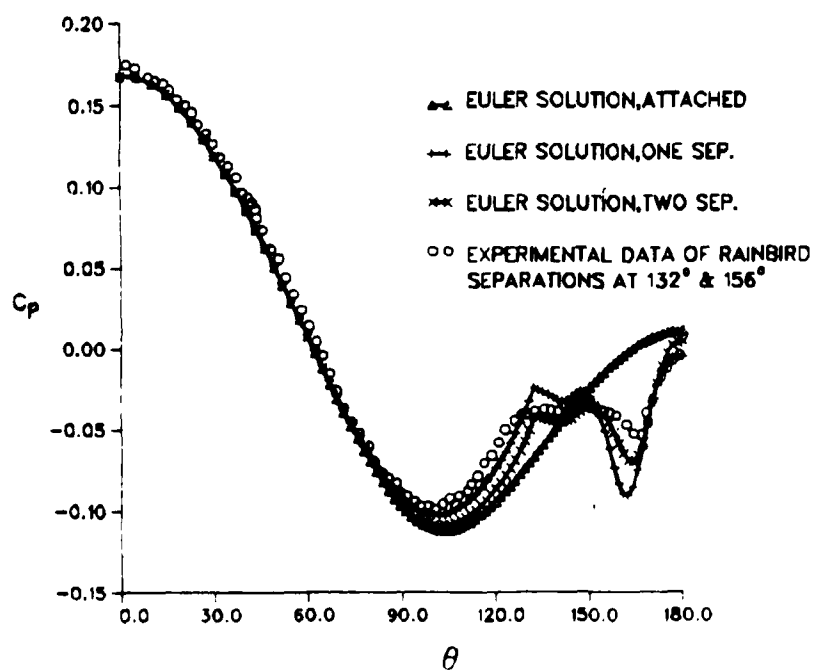


Fig. 27 Surface Pressure Comparison ($M_\infty = 1.79$,
 $\delta = 5^\circ$, $\alpha = 12.65^\circ$)

pressure variation because of the difficulties already mentioned. It is the recompression between $\theta = 162^\circ$ and $\theta = 150^\circ$ which causes secondary separation. With secondary separation included the expansion/recompression of the reverse flow is reduced and the computed results in this region approach the experimental data. The pressure plateau between primary separation ($\theta = 132^\circ$) and $\theta = 150^\circ$ becomes flatter and its level is very close to the experimental data. The inclusion of secondary separation moves the pressure distribution before primary separation away from the experimental data. This is due to the flattening of the vortex sheet discussed previously. Some of the differences between the experimental data and the computed results are surely due to viscous effects (i.e., boundary layer thickening before separation). This is true for both primary and secondary separation. It should be pointed out that the experimental separation is not at the beginning of the plateau in the experimental pressure. This is not typical of purely inviscid separation indicating a significant boundary layer thickening in this case.

The next case considered was at a lower angle of attack 10.6° (5° cone at $M_\infty = 1.79$). The surface pressures are shown in Fig. 28. The separations are at $\theta = 139^\circ$ and 157° . The behavior is similar to that shown in Fig. 27. In this case the inclusion of secondary separation brings the surface pressure compression upstream of separation back to essentially the attached results. The reason for this becomes obvious after a comparison of crossflow streamlines with and without secondary separation (Fig. 29 & 30). The pressure plateau in this case is very flat. A large discrepancy between calculation and experimental data in the reverse flow region is eliminated with the inclusion of secondary separation. While the inclusion of secondary separation does bring the calculated results closer to the experimental data in the reverse crossflow region, it seems obvious that viscous effects are important there; the experimental data show this. In the subsonic crossflow cases considered thus far, any viscous effects which modify the vortex core location can effect the global solution. The discrepancies between calculated results and experimental data before primary separation are totally eliminated when supersonic crossflow is considered.

The last case to be considered involves supercritical crossflow. It is the high speed ($M_\infty = 4.25$) flow over the same 5° cone at $\alpha = 12.35^\circ$.

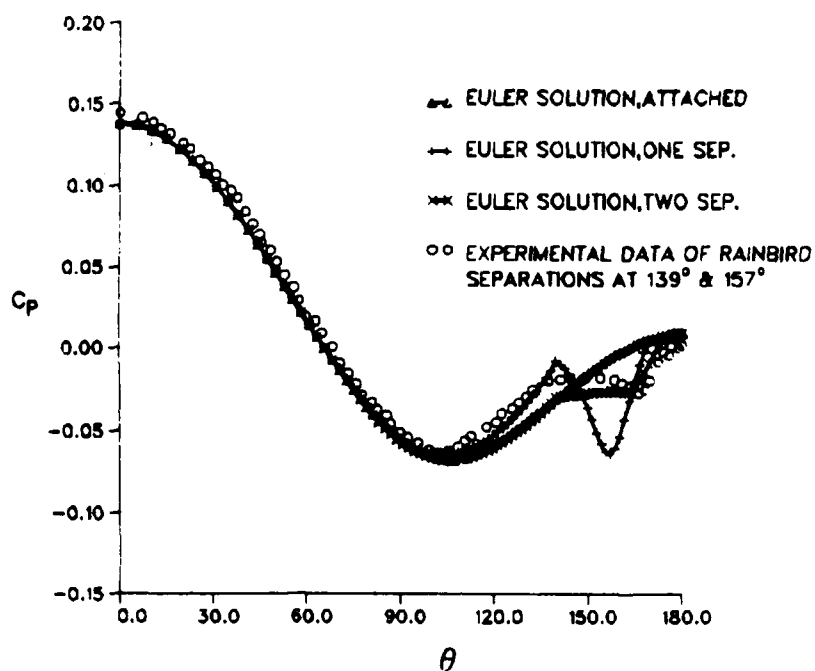


Fig. 28 Surface Pressure Comparison ($M_\infty = 1.79$, $\delta = 5^\circ$, $\alpha = 10.6^\circ$)

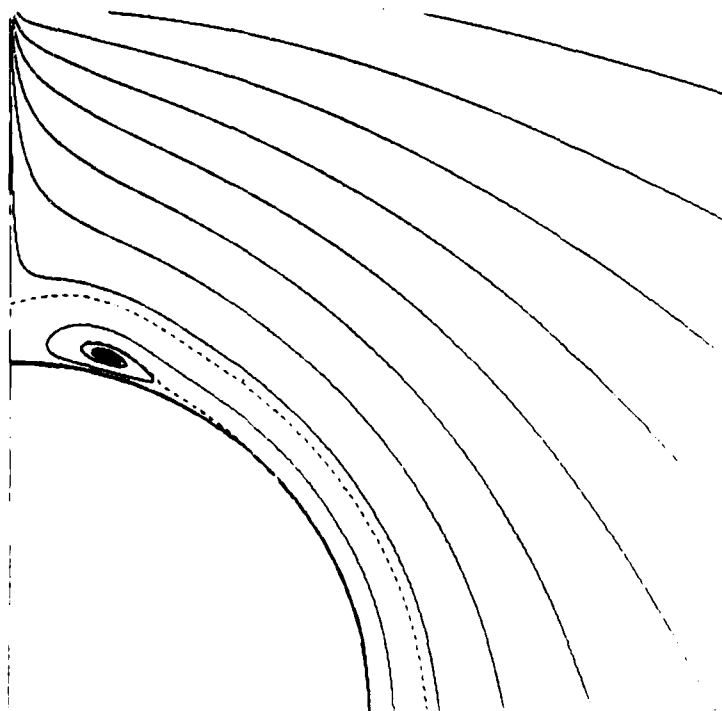


Fig. 29 Crossflow Streamlines, Primary & Secondary Separations ($M_\infty = 1.79$, $\delta = 5^\circ$, $\alpha = 10.6^\circ$)

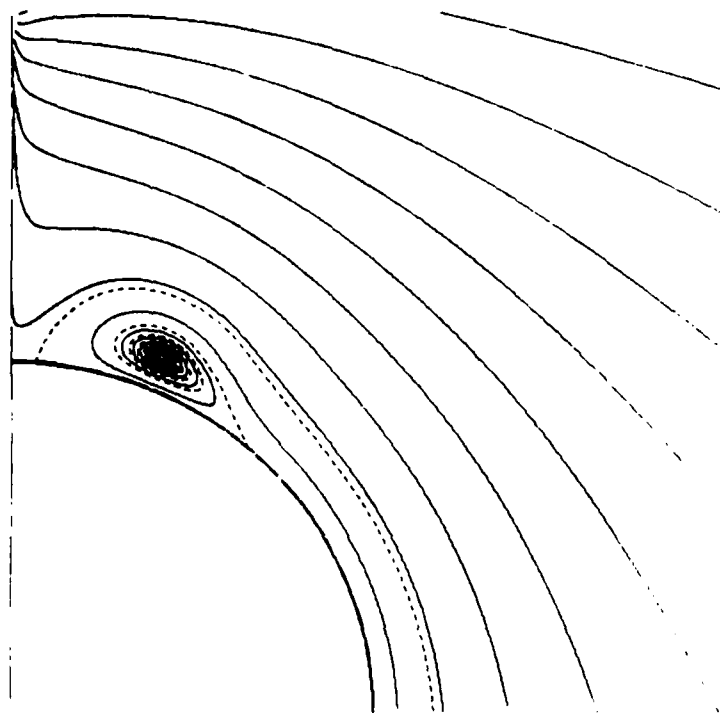


Fig. 30 Crossflow Streamlines, Primary Separation
 ($M_\infty = 1.79$, $\delta = 5^\circ$, $\alpha = 10.6^\circ$)

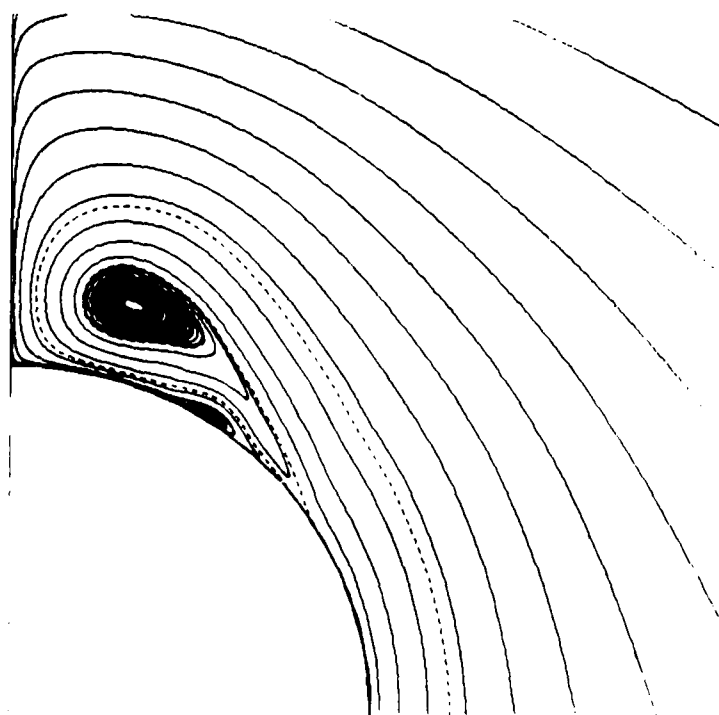


Fig. 31 Crossflow Streamlines, Forced Primary
 Separation Shock Induced Secondary Separation
 ($M_\infty = 4.25$, $\delta = 5^\circ$, $\alpha = 12.35^\circ$)

The streamlines for this case are very interesting. Figure 31 shows the streamlines with primary separation forced at $\theta = 120^\circ$ and no secondary separation forced. The vortex very close to the body is a result of a shock induced separation at $\theta \approx 151^\circ$. With only primary separation specified (i.e., shedding vorticity) the reverse crossflow becomes supersonic causing a reverse crossflow shock. This shock can be seen from the isobars of Fig. 32 ($\theta \approx 154^\circ$). It is the vorticity generated by this shock which causes the secondary separation in Fig. 31. An oblique crossflow shock is apparent from the isobars of Fig. 32 at the primary separation point. This is due to the fact that the sheet comes off at an angle relative to the body as discussed previously. The dashed line off the surface at $\theta = 90^\circ$ (Fig. 31) wraps around the vortex and stagnates at a saddle on the surface. This streamline partitions the flow which goes into the main vortex node from that which spirals into the secondary vortex node.

Figure 33 shows the streamlines for this case with both primary and secondary ($\theta = 160^\circ$) separations specified. The figure shows a third vortex near the primary vortex sheet. The streamlines passing over the secondary vortex pinch together to form a saddle just above the secondary vortex. The existence of this saddle implies the formation of an additional node which is the spiral node close to the vortex sheet just after separation. The shock system in this case is quite complex and can be deduced from the isobars of Fig. 34. An oblique crossflow shock can be seen leaving the surface at the primary separation point, this shock becomes normal to the flow off the body. Visualization of this flow is aided by a look at the crossflow sonic lines (Fig. 35). The sonic line leaving the surface at the separation point coincides with the vortex sheet. The normal portion of the oblique shock formed at the primary separation points can to seem as the supersonic to subsonic transition off the body just after separation ($\theta \approx 132^\circ$). There is another transition further downstream ($\theta \approx 146^\circ$), a corresponding shock can be seen in the isobars of Fig. 34. It seems that the flow then re-expands to supercritical, and this region is terminated by yet another shock ($\theta \approx 165^\circ$). As usual the reverse flow expands as it moves from the lee plane. The reverse crossflow becomes supercritical just beneath the primary vortex ($\theta \approx 165^\circ$). There is then the possibility of an oblique crossflow shock at the secondary separation point. However, the reverse crossflow Mach number is too low to make the deflection required by secondary separation. A

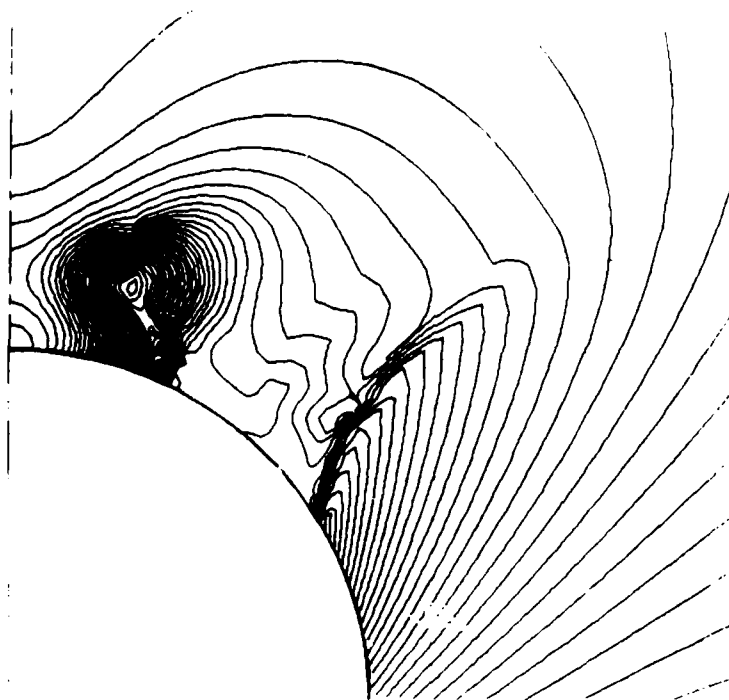


Fig. 32 Isobars, Forced Primary Separation, Shock Induced Secondary Separation ($M_\infty = 4.25$, $\delta = 5^\circ$, $\alpha = 12.35^\circ$)

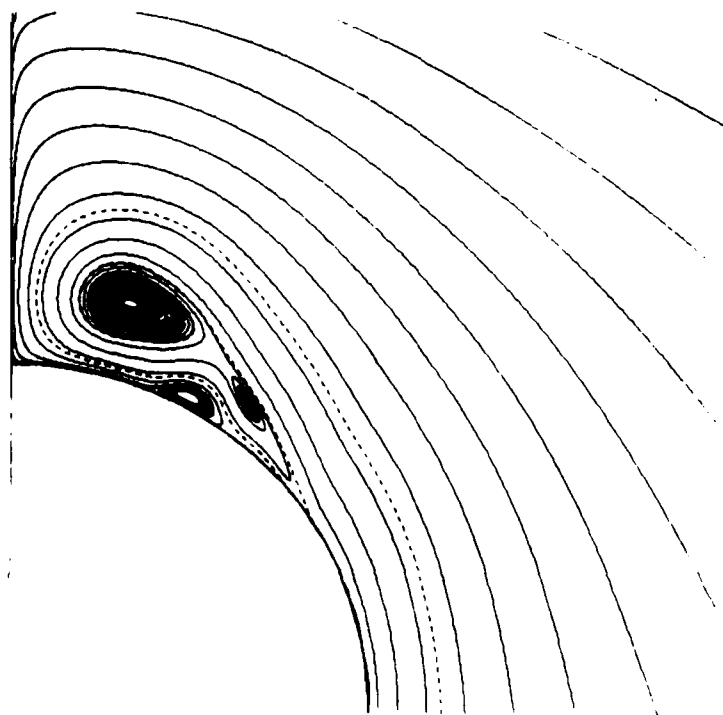


Fig. 33 Crossflow Streamlines, Forced Primary and Secondary Separations ($M_\infty = 4.25$, $\delta = 5^\circ$, $\alpha = 12.35^\circ$)

detached normal shock can be seen before the secondary separation point in both the isobars (Fig. 34) and the sonic line (Fig. 35).

The comparison with the experimental data in this case is much better than those of the two subsonic cases studied previously. The primary vortex core location is computed to be $\theta = 164^\circ$ and $h = 0.22$ which compares very well with Rainbird's data $\theta = 165^\circ$ and $h = 0.23$. More importantly the surface pressure distributions (Fig. 36) compare very well. Figure 36 shows no upstream influence before the primary separation point, a comparison with the attached flow (no forced separation) of Fig. 12 shows no change before $\theta = 120^\circ$. Of course, this is not surprising for the inviscid calculation since the crossflow is supersonic. The surprising result is that the experimental data shows no influence of boundary layer thickening. The pressure rise due to the shock at primary separation compares very well with data, note how sharply the experimental pressure raises. In the region of secondary separation the comparison is somewhat poor. It is becoming quite clear that the flow in this region is influenced significantly by viscous effects. The inclusion of secondary separation moves the compression from $\theta \approx 152^\circ$ to $\theta = 160^\circ$ but the supersonic reverse crossflow is not eliminated. It should be pointed out that the expansion/recompression just after the secondary separation ($\theta \approx 150^\circ$) is consistent with the magnitude of the secondary vortex.

The procedures used to shed vorticity from the surface of a circular cone were applied to the flow about an elliptic delta wing tested by Squire²⁴. The grid used had 89×89 points in cross section and the residual was reduced five orders of magnitude. While Squire didn't determine precisely the primary separation point location, his experimental data indicated leading edge separation for the ellipse ($a/b \approx 14/1$) at $M_\infty = 2$ and $\alpha = 10^\circ$. The computed attached flow surface pressure is shown in Fig. 18. There is a small vortex ($X/X_{LE} \approx .3$) due solely to shock vorticity in the result of Fig. 18. Figure 18 shows a rapid expansion around the wing leading edge followed by a weak recompression before the shock. In the present study it was found that no solution could be obtained with vorticity being shed in the region of favorable pressure gradient near the wing leading edge. Once the weak recompression was reached, separation could be forced to occur. Figure 37 shows the computed surface pressure distribution on the elliptic delta wing

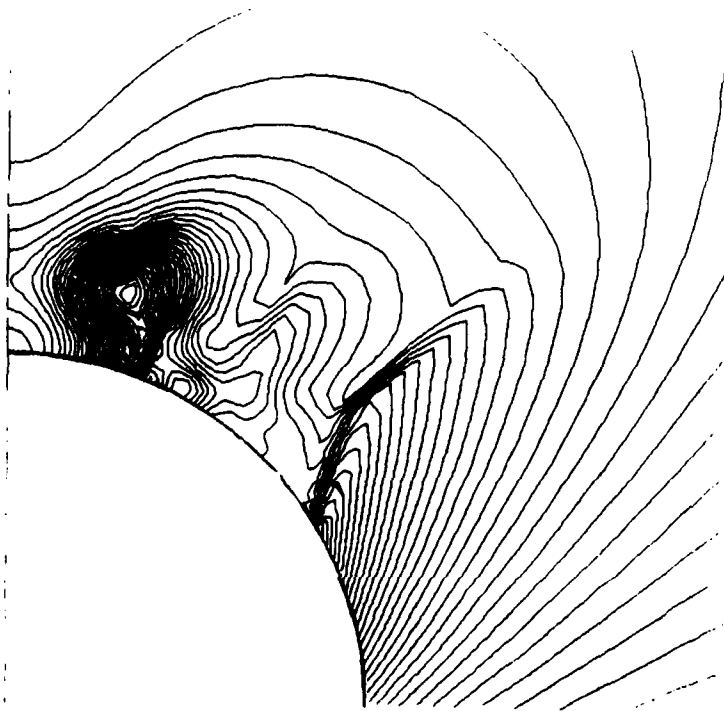


Fig. 34 Isobars, Forced Primary and Secondary Separations ($M_\infty = 4.25$, $\delta = 5^\circ$, $\alpha = 12.35^\circ$)

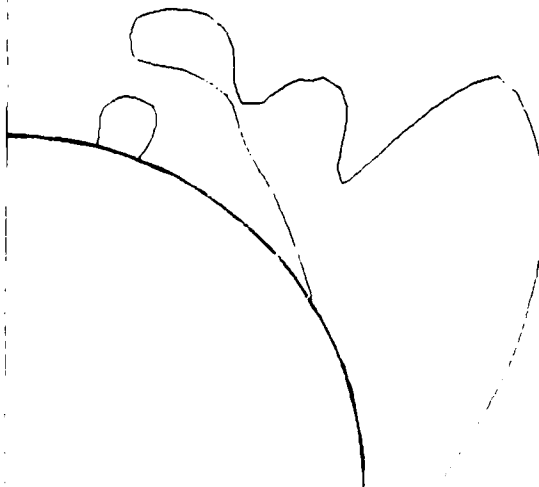


Fig. 35 Crossflow Sonic Lines, Forced Primary and Secondary Separations ($M_\infty = 4.25$, $\delta = 5^\circ$, $\alpha = 12.35^\circ$)

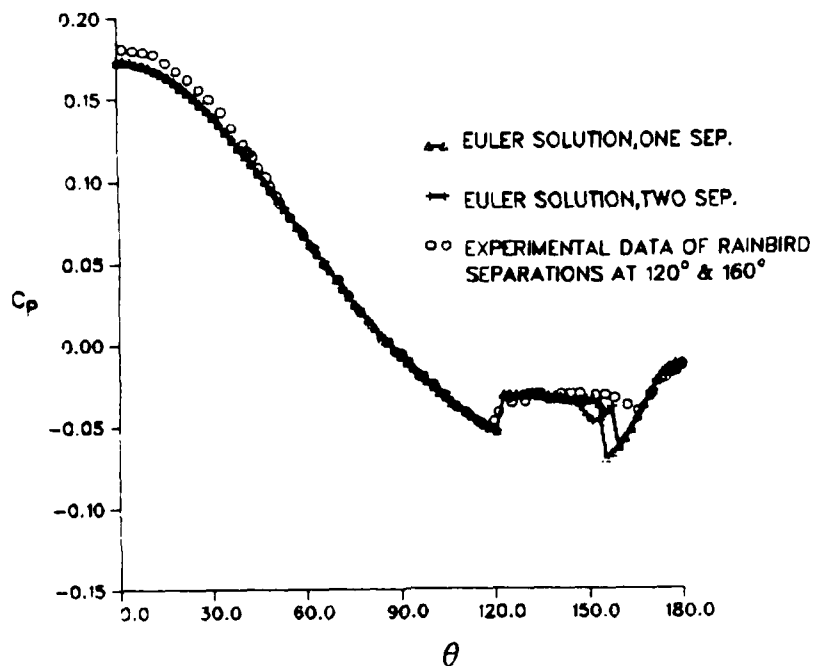


Fig. 36 Surface Pressure Comparison
 $(M_\infty = 4.25, \delta = 5^\circ, \alpha = 12.35^\circ)$

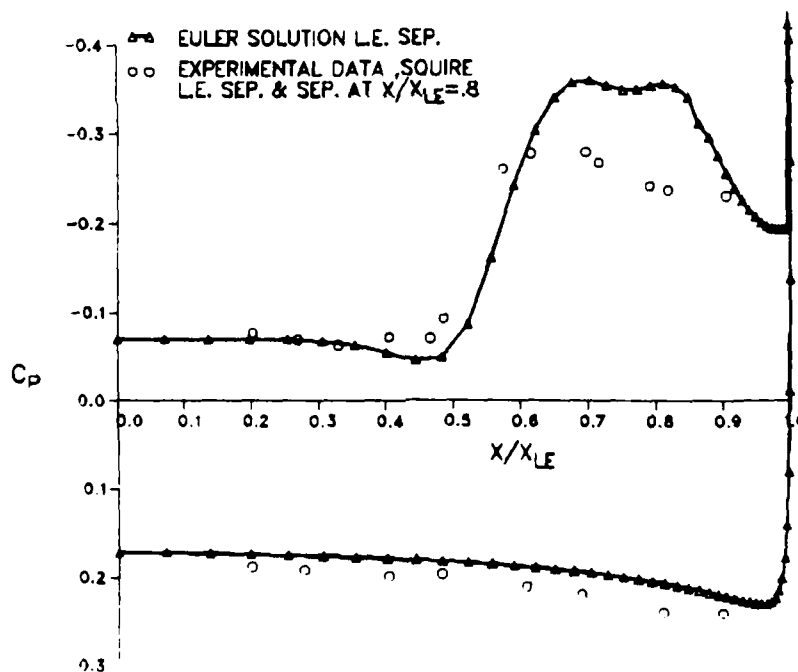


Fig. 37 Surface Pressure Comparison $(M_\infty = 2, \alpha = 10^\circ, 14:1 \text{ Ellipse}, \delta = 1.5^\circ, \lambda = 70^\circ)$ Separation Forced at $X/X_{LE} = .99$

with separation forced at $X/X_{LE} = .99$. (This is as close to the leading edge as possible that separation could be forced.) Figure 37 shows that the flow expands around the leading edge before the specified separation point. In fact this separation is of the supercritical type discussed previously. An oblique shock causes the recompression just after the leading edge compression. Figure 37 also shows the experimental data of Squire²⁴. The comparison is good except for the pressure plateau between $X/X_{LE} = .6$ and $.9$, where secondary separation was detached experimentally. Figures 38 and 39 show the cross-sectional stream-lines and isobars, respectively. A comparison of Fig. 37 and 38 shows that the apparent pressure raise at $X/X_{LE} = .55$ is in the reverse crossflow region, so that it is in reality an expansion on the wing surface. A comparison of Fig. 38 and 39 shows a crossflow shock located above the reverse flow region at $X/X_{LE} \approx .6$. It is this shock's interaction with the reverse crossflow that causes the expansion at $X/X_{LE} \approx .55$. The experimental results indicate secondary separation at $X/X_{LE} = .8$. Figure 40 shows the computed surface pressure distribution with both primary and secondary separation specified (secondary separation is specified at the experimental location). The inclusion of secondary separation brings the pressure level just after primary separation ($X/X_{LE} = .9$ to $X/X_{LE} = 1.$) to the experimental value. The reverse cross is supersonic after the expansion at $X/X_{LE} = .55$, so that the inclusion of secondary separation cannot affect the pressure level between $X/X_{LE} = .6$ and $.8$ and so there is a significant difference between the computed and experimental pressure level in this region. There is shocking of the reverse crossflow at the secondary separation point $X/X_{LE} = .8$ followed by a local minimum in pressure ($X/X_{LE} \approx .85$) under the core of the secondary vortex. The streamline pattern is shown in Fig. 41.

The results of the investigation of the delta wing flow field are the same as those for the circular cone. In particular, it was found that secondary separation is dominated by viscous effects, and an inviscid model (as the one used here) will have difficulties predicting details of the flow in this region. The region of the flow between $X/X_{LE} = .55$ and $.8$ in Fig. 39 is similar to the reverse crossflow region $\theta \approx 170^\circ$ to 140° in Fig. 37 (supercritical cone). In the case of the ellipse this region is longer because the vortex is elongated.

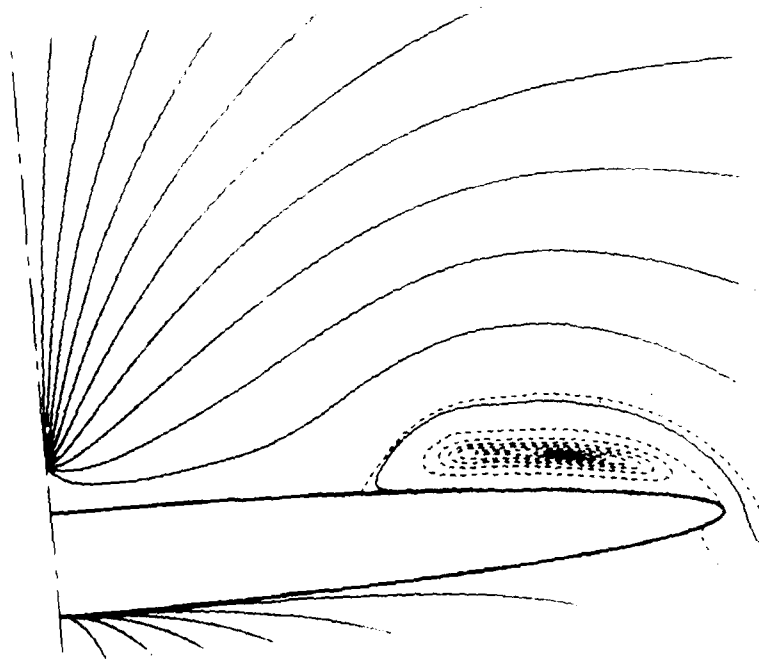


Fig. 38 Crossflow Streamlines ($M_\infty = 2$, $\alpha = 10^\circ$,
14:1 Ellipse, $\delta = 1.5^\circ$, $\lambda = 70^\circ$) Separation
Forced at $X/X_{LE} = .99$

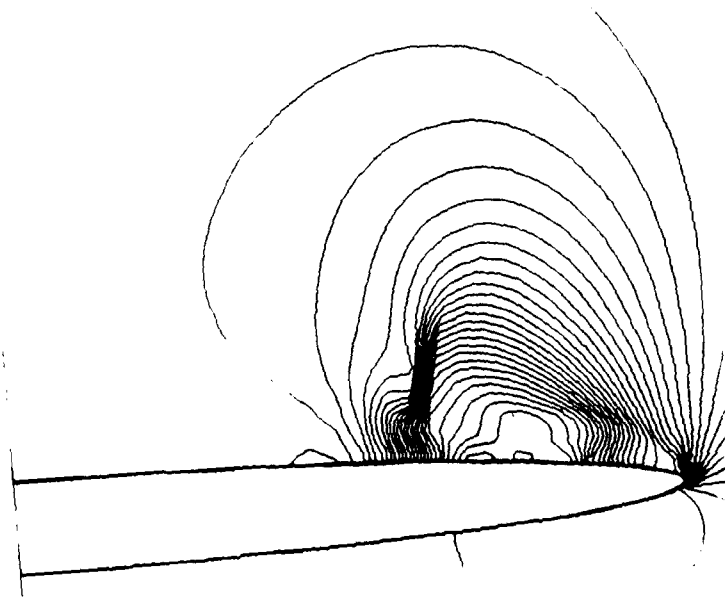


Fig. 39 Isobars ($M_\infty = 2$, $\alpha = 10^\circ$, 14:1 Ellipse,
 $\delta = 1.5^\circ$, $\lambda = 70^\circ$) Separation
Forced at $X/X_{LE} = .99$

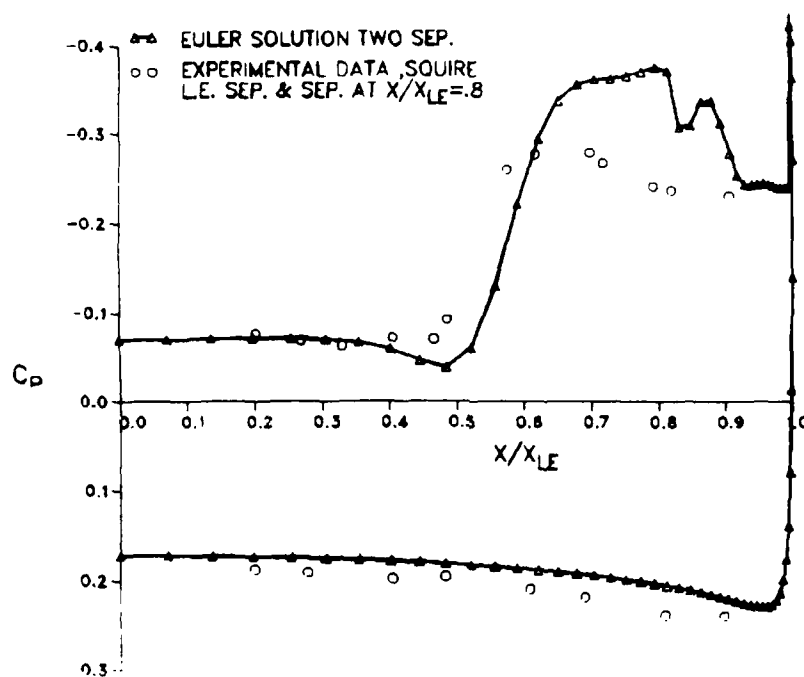


Fig. 40 Surface Pressure Comparison ($M_\infty = 2$, $\alpha = 10^\circ$, 14:1 Ellipse, $\delta = 1.5^\circ$, $\lambda = 70^\circ$) Separation Forced at $X/X_{LE} = .99$ and $X/X_{LE} = .8$

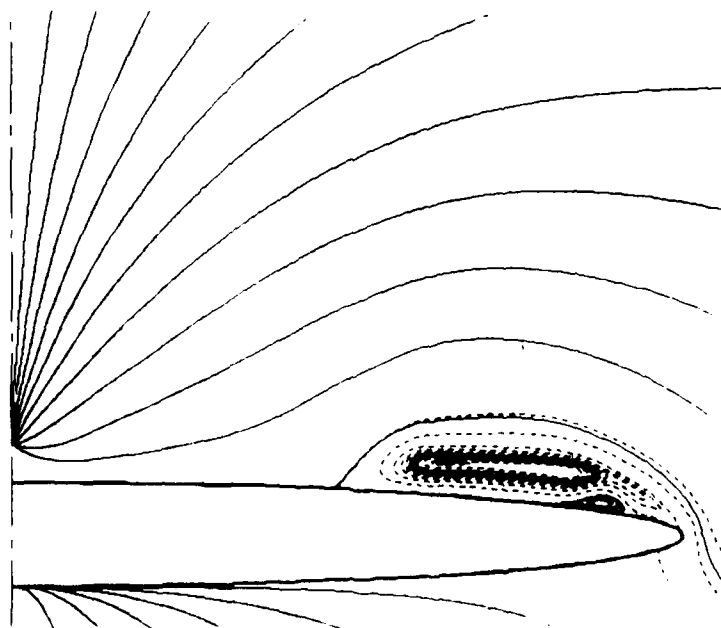


Fig. 41 Crossflow Streamlines ($M_\infty = 2$, $\alpha = 10^\circ$, 14:1 Ellipse, $\delta = 1.5^\circ$, $\lambda = 70^\circ$) Separation Forced at $X/X_{LE} = .99$ and $X/X_{LE} = .8$

6. COMPARISON OF SHOCK VORTICITY & SHED VORTICITY

In an effort to gain a better understanding of the relationship between shock vorticity and vorticity shed from the surface of a smooth body, the flow about the 5° cone tested by Rainbird²² was computed with a number of different separation point locations specified. The case considered was $M_\infty = 4.25$ and $\alpha = 12.35^\circ$. As indicated previously, this flow is supercritical and, with no vorticity shed from the cone surface, the crossflow shock produces enough vorticity to cause separation. Figures 42 and 43 show the crossflow streamlines and isobars, respectively, for this flow with no vorticity shed from the body. Separation for this case is computed to be at $\theta = 151.3^\circ$. Figure 42 indicates that the separating streamlines leave the surface at a large angle (57°) relative to it. As shown earlier in this paper (Fig. 5), when only shock vorticity is present there is no jump in crossflow velocity at the separation point, which is consistent with the fact that no vorticity is being shed from the surface. It should be pointed out that in the computational results that follow, all crossflow shocks are captured. Figure 43 indicates that the shock is captured very sharply (see the closely spaced isobars). Additionally, these captured shock results compare very well with the shock fit results for this case (Fig. 12).

Figures 44 and 45 show results for the other extremes of separation point location studied ($\theta = 115^\circ$). Figure 44 shows the crossflow streamlines. The secondary separation shown is due to a strong reverse crossflow shock (see Fig. 45), and the third vortex off the surface is similar to the one discussed previously. In Fig. 45, the isobars are shown, and they indicate an oblique shock at the specified primary separation point. The jump in velocity at the separation point is significant with separation specified at $\theta = 115^\circ$, indicating significant vorticity being shed from the surface. A comparison of Fig. 42 and 44 shows that the extent of the vortical regions are comparable, while the two sources of vorticity are very different.

The relationship between shock vorticity and shed vorticity is made clearer by considering Fig. 46. The figure shows the jump in crossflow velocity vs separation point location. The jump in crossflow velocity is directly related to the vorticity shed into the flow field from the separation point. The shock configuration transition from an oblique crossflow shock to

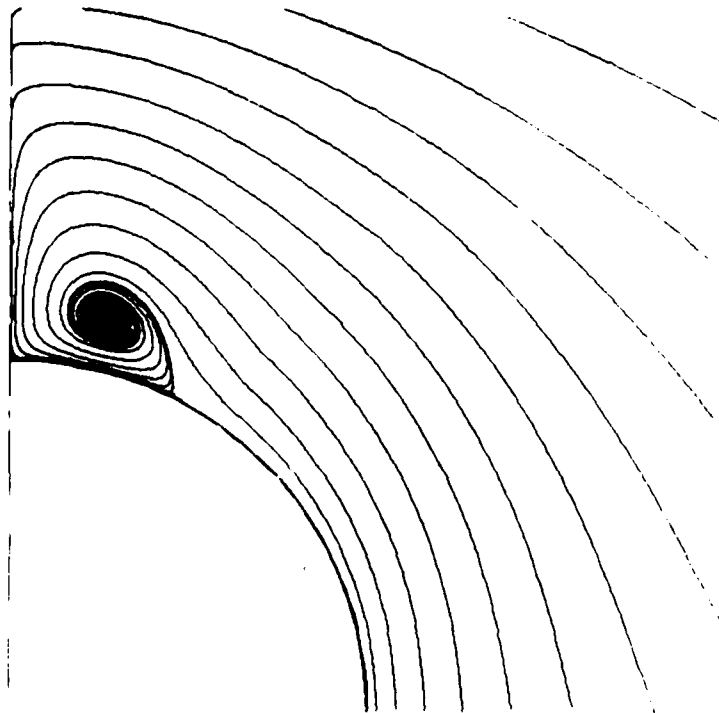


Fig. 42 Crossflow Streamlines on the 5° Circular Cone ($M_\infty = 4.25$, $\alpha = 12.35^\circ$) Separation Due to Shock Vorticity Alone at $\theta = 151.3^\circ$

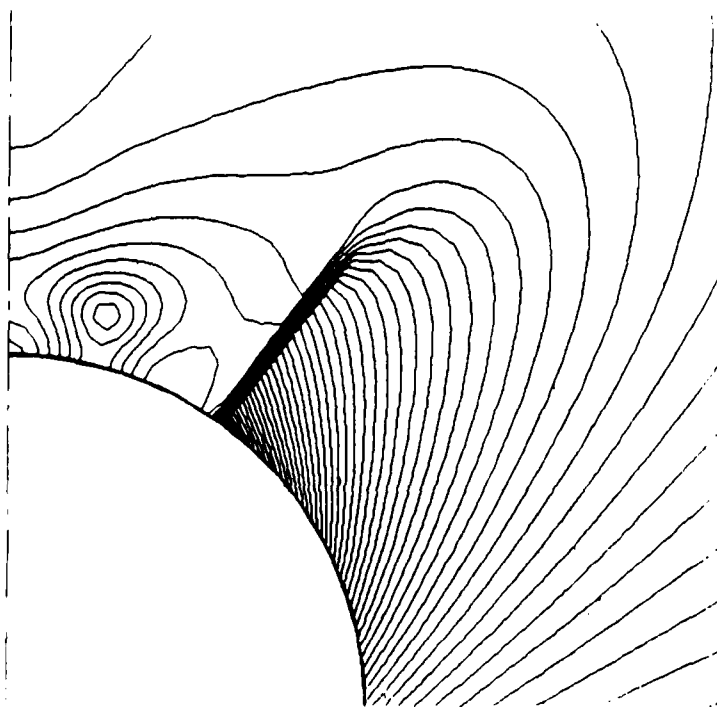


Fig. 43 Isobars on the 5° Circular Cone ($M_\infty = 4.25$, $\alpha = 12.35^\circ$) Separation due to Shock Vorticity Alone at $\theta = 151.3^\circ$

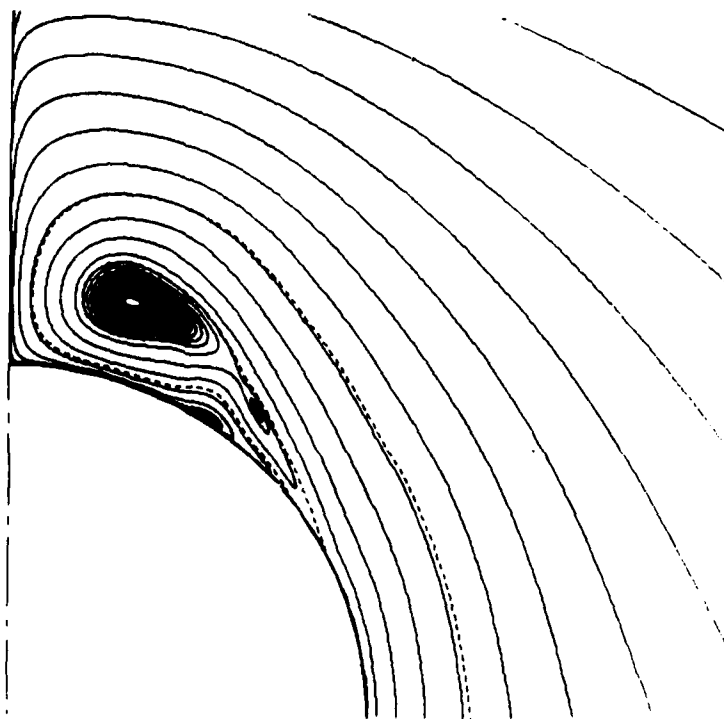


Fig. 44 Crossflow Streamlines on the 5° Circular Cone ($M_\infty = 4.25$, $\alpha = 12.35^\circ$) Separation Forced at $\theta = 115^\circ$

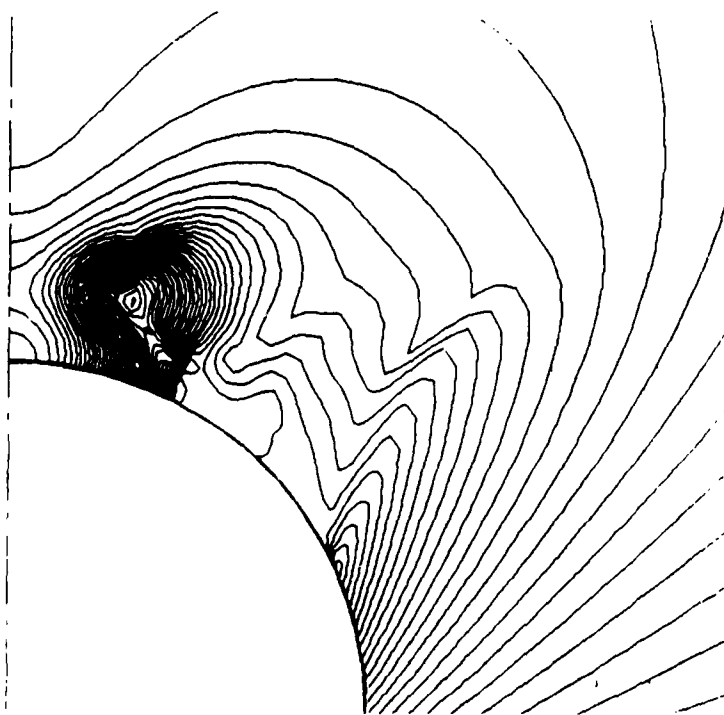


Fig. 45 Isobars on the 5° Circular Cone ($M_\infty = 4.25$, $\alpha = 12.35^\circ$) Separation Forced at $\theta = 115^\circ$

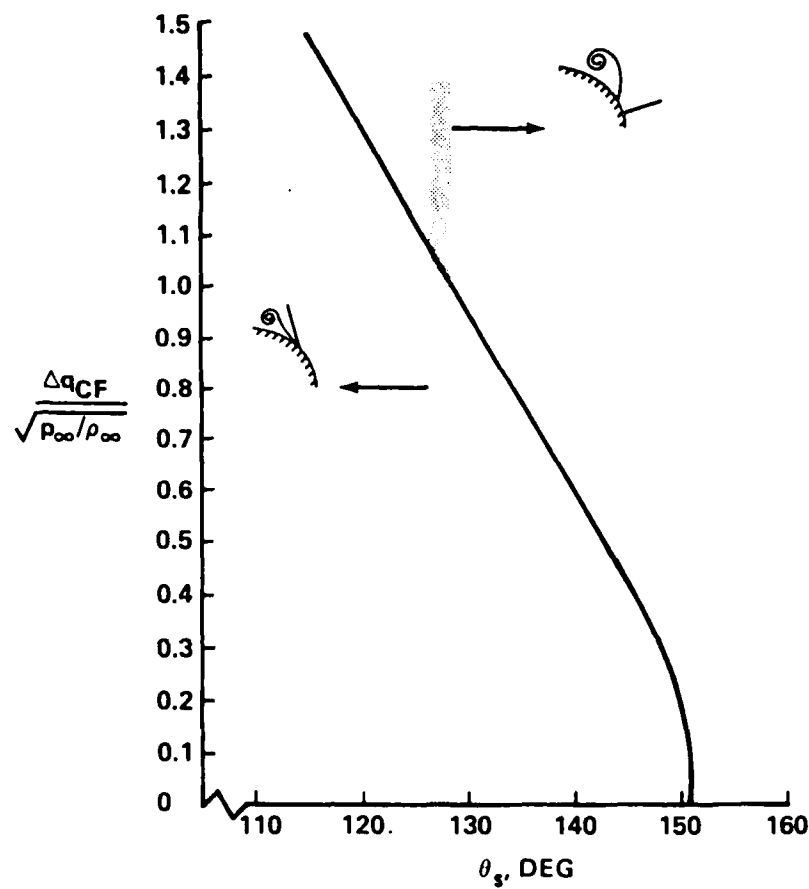


Fig. 46 Vorticity Shed into the Flow Field as a Function of Separation Point Location

a detached normal crossflow shock occurs at about $\theta_s \approx 128^\circ$ (indicated by the shaded area in Fig. 46). It should be pointed out that the jump in velocity at the separation point in the oblique shock cases was computed by subtracting the oblique shock velocity jump from the numerical results. Thus, the jumps in velocity in Fig. 46 represent the jumps across the vortex sheet at separation. The figure shows that this velocity jump goes to zero smoothly as the separation point location due to shock vorticity alone is approached ($\theta_s = 151.3^\circ$). This indicates that separation due to shock vorticity alone and that due to shed vorticity are related. In fact, it would seem that separation due to shock vorticity alone is a particular solution of the set of solutions in which vorticity is shed from the surface. In this particular solution the value of the vorticity shed is zero.

6. CONCLUSIONS

The research effort in this area is ongoing, and while some of the results presented here should be considered preliminary, a number of conclusions have been reached:

- o The vorticity produced by the shock system in supersonic conical flow can cause separation on its own and may add significantly to the vorticity shed from a separating boundary layer
- o As the shock system becomes weak and approaches a potential (i.e., irrotational) shock, its vorticity no longer causes separation (Fig. 8)
- o The reverse crossflow can become supersonic beneath a vortex core and a reverse crossflow shock may form (Fig. 10 & 11). This shock can cause secondary separation on its own (Fig. 31)
- o Increasing eccentricity on elliptic cross sections has a tendency to reduce shock entropy gradients and thus vorticity. Yet, the separation caused by shock vorticity can have a significant impact on the flow field (Fig. 22)
- o The artificial damping required to stabilize captured shocks does not necessarily significantly distort shock vorticity (Fig. 18)
- o Both primary and secondary separation can be forced at specified locations by shedding vorticity from a smooth surface. With the vorticity shedding model of Smith⁵, the basic features of the separated flow can be reproduced
- o Euler calculations including vorticity shedding are more accurate and in some sense simpler than those using irrotational flow models

- o There are computational difficulties in a small region after separation that may significantly affect the global results
- o In the case of supercritical crossflow, the vortex sheet leaves the surface at an angle relative to it causing an oblique crossflow shock (Fig. 31 to 35)
- o The viscous effects (boundary layer thickening) upstream of separation are much more significant in the case of subsonic crossflow than in the case of supercritical crossflow (Fig. 27 & 36)
- o Secondary separation is influenced more by viscous effects than primary separation
- o The vorticity shed into the flow field is reduced smoothly as the separation point is moved to its shock induced location (Fig. 46).

7. REFERENCES

1. Küchemann, D., "Inviscid Shear Flow Near the Trailing Edge of an Aerofoil," R.A.E. TR 67068 (1967).
2. Fraenkel, L.E., "On Corner Eddies in Plane Inviscid Shear Flow," J Fluid Mechanics, Vol 11, pp 400-406 (1961).
3. Smith, P.D., "A Note on the Computation of the Inviscid Rotational Flow Past the Trailing Edge of an Airfoil," R.A.E. TM 1217 (1970).
4. Smith, J.H.B., "Remarks on the Structure of Conical Flow," Progress in Aeronautical Sciences, Vol 12, pp 241-271 (1972).
5. Smith, J.H.B., "Behavior of a Vortex Sheet Separating from a Smooth Surface," R.A.E. TR 77058 (1977).
6. Fiddes, S.F., "A Theory of the Separated Flow Past a Slender Cone at Incidence," AGARD CP 291, pp 30-1 - 30-14 (1981).
7. Marconi, F., "The Spiral Singularity in the Supersonic Inviscid Flow Over a Cone," AIAA Paper 83-1665 (1983).
8. Salas, M.D., "Recent Developments in Transonic Euler Flow Over a Circular Cylinder," NASA TM 83282 (1982).
9. Rizzi, A., Erickson, L., Schmidt, W. and Hitzel, S., "Numerical Solutions of the Euler Equations Simulating Vortex Flows Around Wings," AGARD CP-342, pp 21-1 - 21-14 (1983).
10. Murman, E., "Solutions of the Conical Euler Equations for Flat Plate Geometries - Preliminary Results," MIT CFDL-TR-84-4 (1984).
11. Newsome, R., "A Comparison of Euler and Navier-Stokes Solutions for Supersonic Flow Over a Conical Delta Wing," AIAA Paper 85-0111 (1985).
12. Marconi, F., "Supersonic Conical Separation Due to Shock Vorticity," AIAA J, Vol 22, No. 8, pp 1048-1055 (1984).
13. Marconi, F., "Shock Induced Vortices on Elliptic Cones in Supersonic Flow," AIAA Paper No. 85-0433 (1985).
14. Marconi, F., "Supersonic Inviscid, Conical Corner Flow Fields," AIAA J, Vol 18, No. 1, pp 78-84 (1980).
15. Moretti, G., "The λ -Scheme," Computers and Fields, Vol 7, pp 191-205 (1979).
16. Marconi, F., Salas, M.D. and Yaeger, L., "Development of a Computer Code for Calculating the Steady Super/Hypersonic Inviscid Flow Around Real Configurations," NASA CR-2675 (1976).

17. Rudman, S., "Multinozzle Plume Flow Fields - Structure and Numerical Calculations," AIAA Paper 77-710 (1977).
18. deNeef, T. and Moretti, G., "Shock Fitting for Everybody," Computers and Fluids, Vol 8, pp 327-334 (1980).
19. Vorropoulos, G. and Wendth, J. F., "Laser Velocimetry Study of Compressibility Effects on the Flow Field of a Delta Wing," AGARD CPP-342 (1983).
20. Nielsen, J.N., Kuhn, G.D., and Klopfer, G.H., "Euler Solutions of Supersonic Wing-Body Interference at High Incidence Including Vortex Effects," NEAR TR 263 (1982).
21. Siclari, M. and Visich, M., "Shock Fitting in Conical Supersonic Full Potential Flows with Entropy Effects," AIAA Paper 84-0261 (1984).
22. Rainbird, W.J., "The External Flow Field About Yawed Circular Cones," AGARD CP30 (1968).
23. Siclari, M.J., "Supersonic Nonlinear Potential Flow with Implicit Isentropic Shock Fitting," AIAA J, Vol 20, No. 7, p 924 (1982).
24. Squire, L.C., "Leading-Edge Separations and Cross-Flow Shocks on Delta Wings," AIAA J, Vol 23, No. 3, p 321 (1985).

END

1-87

DTIC

